Politecnico Di Milano

School of arquitecture urban planning and construction engineering

Master of Science in Building and Architectural Engineering

BOND BEHAVIOR OF FIBER REINFORCED CEMENTITIOUS MATRIX (FRCM) COMPOSITES: EFFECT OF THE STRESS REDISTRIBUTION

Professor Carlos Poggi
Tutor: Tommaso D´Antino

Elaborated by
Carlos Hidalgo – 862789

Academic Year 2017/2018

Acknowledgements

Throughout the human history, the continuous improvement and important achievements towards the development of us as a society, have been carried out thanks to the continuous learning process linked to the different demands and needs during the human existence. Nowadays, I strongly believe that the constant learning motivated and addressed to a common end is the way how we, as a collective force, can developed ourselves. Reason why I want to acknowledge the different people who during the last time were enhancing and driving this process alongside with me, being the necessary support to reach a successful ending. Regarding the academic field, I would like to express my special gratefulness to Professor Carlos Poggi and Tommaso D´Antino, who continuously coached me and helped me on every single step taken making possible this final achievement.

My family, on the other hand, has played a special and underlying role being the driving force carrying with it the energy source during this personal and professional process, belonging to them the major part of this final achievement. Not forgetting of course, my sentimental partner, person who has been playing as my teammate, backing me up when was necessary reaching the end together.

En memoria de Rosario Baranza.

Abstract

Lately Fiber Reinforced Cementitious Materials (FRCM) have been widely spread within seismic-resistant reinforced techniques, in which its applicability due to its compatibility with various substrates is one of its outstanding features. This retrofitting technique consists of certain dry fibers embedded in an inorganic matrix, gaining with this a raise in the ultimate tension strength. Its applicability regarding the historical buildings, carrying with it an important heritage value, entails considerable advantages such as reversibility, compatibility with both masonry and concrete substrates and high corrosion resistance.

Within the present job parameters such as the impact on the final strength changing the way of casting, being in some cases done from the top of the specimens and others from the bottom, load distribution among the different bundles of the textile and bond behavior of FRCM in different specimens are studied and furtherly discussed. To do so, two methods were carried out, contact measurement and a non-contact technique being in this case Digital Image Correlation (DIC). The set-up used for this job was shear-bonding test where a tension load is applied on the specimen until the failure, occurring due to the debonding.

The present experimental campaign consists to test six PBO-FRCM specimens and others six using Steel-FRCM, performing the contact measurement analysis for both and DIC only for PBO-FRCM. The final part of the job consists of the discussion of the results and their corresponding comparison, stablishing some considerations for further jobs and guidelines based on the performance observed, leading to the possible generalization of its applicability on field.

Abstract (Italiano)

I materiali cementizi fibrorinforzati (FRCM) hanno avuto un'ampia diffusione nel corso degli ultimi anni come tecnica di rinforzo sismo-resistente; una delle loro caratteristiche più importanti è rappresentata dalla vasta applicabilità dovuta all'elevata compatibilità con vari substrati. Questa tecnica di retrofit consiste nell'incorporare delle fibre secche in una matrice inorganica, ottenendo così un aumento della resistenza a trazione finale. La loro applicabilità ad edifici antichi, che hanno un'importante valore storico, è basata su notevoli vantaggi come la reversibilità, la compatibilità con substrati sia in muratura sia in calcestruzzo ed un'elevata resistenza alla corrosione. In questo lavoro di ricerca vengono analizzati parametri quali l'impatto sulla forza finale del metodo di posa dei campioni, essendo alcuni posati dall'alto ed altri dal basso, la distribuzione di carico tra i diversi fasci di tessuto ed il modo in cui gli FRCM legano nei diversi campioni. Sono state eseguite due tipologie di indagini: la prima è una misurazione a contatto e la seconda è invece una tecnica senza contatto, la correlazione dell'immagine digitale (DIC). Il set-up utilizzato per questa ricerca è rappresentato da prove di taglio in cui viene applicato un carico di tensione sul provino fino al cedimento, che si verifica a causa del distacco della fibra dalla matrice, debonding.

Questa campagna di esperimenti è stata effettuata su sei campioni di tipo PBO-FRCM e su altri sei campioni di Acciaio-FRCM; l'analisi della misurazione a contatto è stata eseguita per entrambe le tipologie di campioni, la DIC solo per i campioni PBO-FRCM. Al termine della presentazione degli esperimenti, segue una discussione sui risultati e vengono tratte alcune considerazioni generali su ulteriori possibili lavori di ricerca e sulla definizione di linee guida per l'eventuale generalizzazione della loro applicabilità in campo.

Table of Contents

Table of figures

List of tables

1. INTRODUCTION AND STATE OF THE ART

1.1. FRCM materials

During the last decades, and due to the number of a considerably earthquakes that took place at center of Italy, the retrofitting and structural rehabilitation have gained important attention, especially in Italy that due to its width spread arquitecture richness, has become susceptible to important structural damages.

The cement-based materials such as concrete due to its nature, has a very low tensile capacity as well as its ductile behaviour, reason why, especially for historical and preserved buildings, exists the imminent need to carry out a strengthening intervention.
Lately, the use of Fiber Reinforced Cementitious Matrix (FRCM) has become popular and well used to fulfill this current aim.
The FRCM can be defined as a structural planar grid composed by a certain number of filaments forming the yarns, constituting the structure able to provide the structural stability intended. Usually the filaments are made mainly by, glass, PBO, carbon or steel.

In addition, FRCM has gained especial attention as a strengthening technique due to its numerous advantages such as physical and chemical compatibility, reversibility, cost and time of installation, especially when the surface to be retrofitted is an irregular building. Therefore, for the specific case of Italy, in which a major percentage of buildings has a valuable historical value, the update process to the current seismic design code is necessary using strengthening techniques having low visible impact.

However, the limited data due to its complex mechanical behaviour, the generalization of the FRCM´s use at a bigger scale has not been possible.
Currently exist an American strengthening guideline titled "*Acceptance criteria for cement-based matrix Fabric Composite System for Reinforced and Unreinforced masonry*" (AC218), "*guide to design and construction of externally bonded fabric reinforced cementitious matrix (FRCM) systems for repair and strengthening of concrete and masonry structures" (*AC1549.4R-13), which provides certain statements to evaluate and characterize the FRCM systems. Moreover, depending on the substrate which will be retrofitted, a different design should be carry out (e.g. clay brick, concrete, etc). thus, the generalization and worldwide application of FRCM as a strengthening technique is still in progress.

1.1.1. Composites materials for strengthening

Composites materials can be defined as the combinations of two or more different materials, and for the specific case of buildings strengthening, the most common used material and well known currently within the engineering field are the fiber composite products. These materials are mainly obtained by embedding or impregnating high strength fibers in an inorganic or organic matrix.

As well as the matrix, the fibers can be organic or inorganic. Currently within the market, inorganic fibers can be made of:

- Glass
- Carbon

While organic fibers are made of:

- Aramid
- Polyvinyalcohol.
- Others.

Despite the wide variety of fibers, for retrofitting interventions, the most commonly type of fibers used are: carbon (CFRP), Aramid (AFRP) and glass (GFRP). The final form of these fibers is according to the final aim and the applicability of each one depending upon the material on which the retrofitting will be made. Additionally, CFRP, AFRP, and GFRP comparing to the steel performance for such purposes, clearly indicate considerable advantages over the use of steel (table 1)

Characteristic	Steel	CFRP	AFRP	GFRP
Tensile Strength	●	●	●	■
Elongation	●	■	■	■
Elastic Modulus	●	■	×	×
Relaxation and Creep	●	●	×	■
Fatigue Strength	●	●	●	●
Alkali Proof	●	●	■	×
Corrosion Resistance	×	●	●	●
Specific Gravity	×	●	●	●
Magnetization	×	●	●	●

●: Excellent, ■: Poor, ×: Bad

Table 1. Features of different textiles used for FRCM. Taken from *(Bianchi)*

Considering the table 1, paying special attention to the corrosion resistance, the field of applicability of the FRCM will go further than the steel´s one, independently for instance of the place where the intervention is needed and its aggressiveness.

The strength of the fibers used, depend mainly upon the type of fiber and its content in the matrix. For retrofitting purposes and such, the desirable mechanical features are:

- High tensile strength.
- High elastic modulus.
- Stability at ambient temperature.

These materials present a set of advantages compared to the traditional strengthening techniques as: lightweight, speed of execution, worthy mechanical characteristics and good performance at failure (Carozzi, 2016).
For the current purpose, the work developed was based on the evaluation of Fabric Reinforced Cementitious Matrix (FRCM), which is a particular type within the textile reinforced concrete. FRCM is constituted by dry-fibers in textile form which are embedded of impregnated in a cementitious mortar. The mortar used, usually has a low content of organic polymers. Although the bonding interaction at mortar/fiber interface and at mortar/substrate interface limits in some cases the intervention, advantages as reversibility of the intervention and durability to external agents enhance its applicability, especially on historical buildings (mostly masonry buildings), due to its compatibility between the substrate and the FRCM.

To carry out a retrofitting intervention, the most commonly fabric used is woven textile composed by yarns passing under and over each other connected by friction (figure 1). However, exist bonded yarns as well.

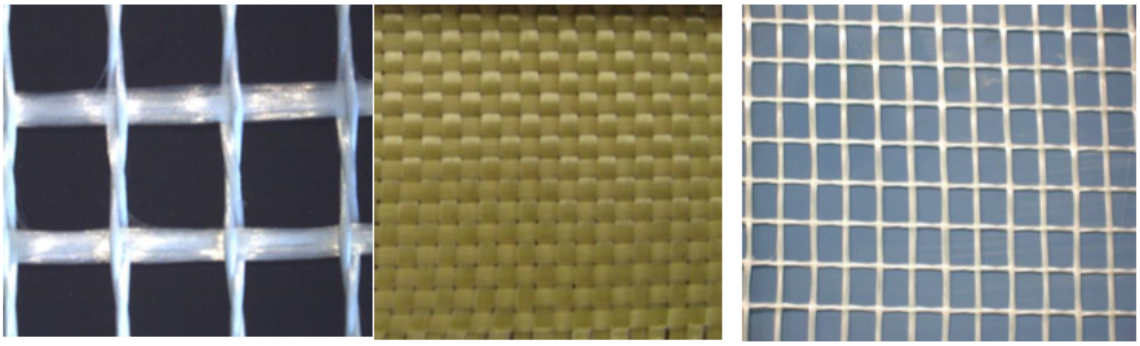

Figure 1 a,b) woven yarns; c) bonded yarns. Taken from *(Carozzi, 2016)*

1.1.2. Materials used

During the characterization of the FRCM systems were tested twelve specimens in total, six using a strengthening material made of Poliparaphenylene benzobisoxazole (PBO) fiber with the

fibers addressed along two orthogonal directions (Fig. 1), and 6 using steel fibers disposed in the same way as the PBO fibers were (Fig. 2).

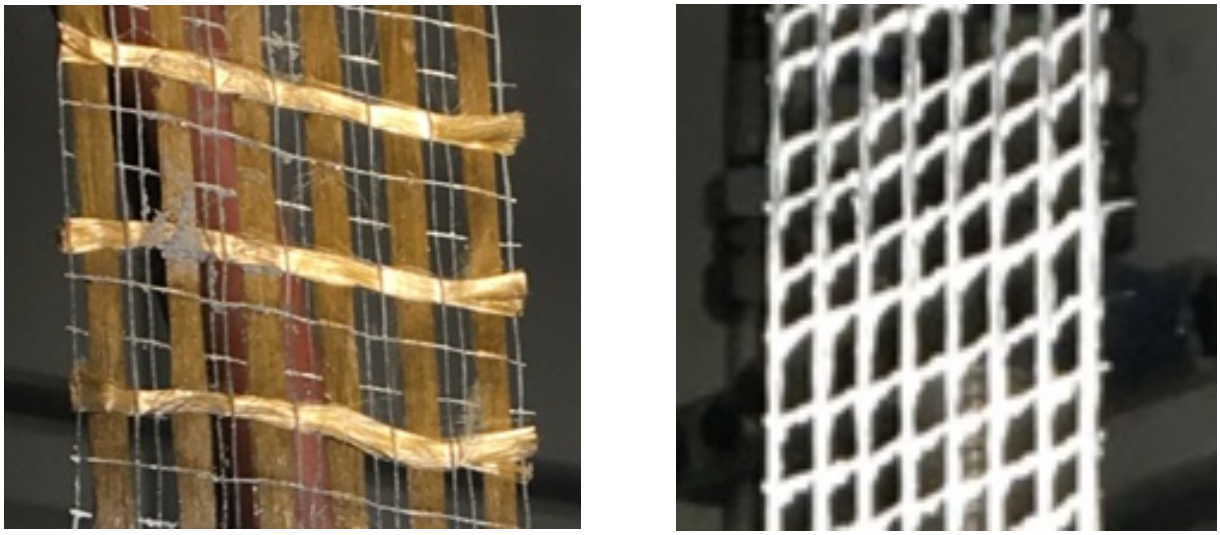

a) B)

Figure 2 a) PBO fibers; B) steel fibers

PBO

The recently increase of use of this materials is owing to their advantages in which the high tensile strength, low weight, high resistance to corrosion and an easy application on field are outstanding features capable of performing a desire retrofitting intervention on masonry and concrete buildings.

The combination of a dry mortar and such performing material as PBO is, result in a raise of the ultimate compressive capacity of the intervened structural element. According to different studies, its results concur demonstrating that the effectiveness of the intervention and application of PBO-FRCM composites is clearly evident on concretes of lower compressive strength. Hence, with the raise of concrete strength, the strengthening effectiveness decreases. According to the results obtained by (Trapko, 2014), the ultimate strength value, once the intervention is carried out, considers the elongation capacity of the PBO fibers. In the figure 3 the results obtained by the author are exposed, showing the impact of the intervention in terms of fi/fu and fcc/fco ratio, where the rise is clearly linear.

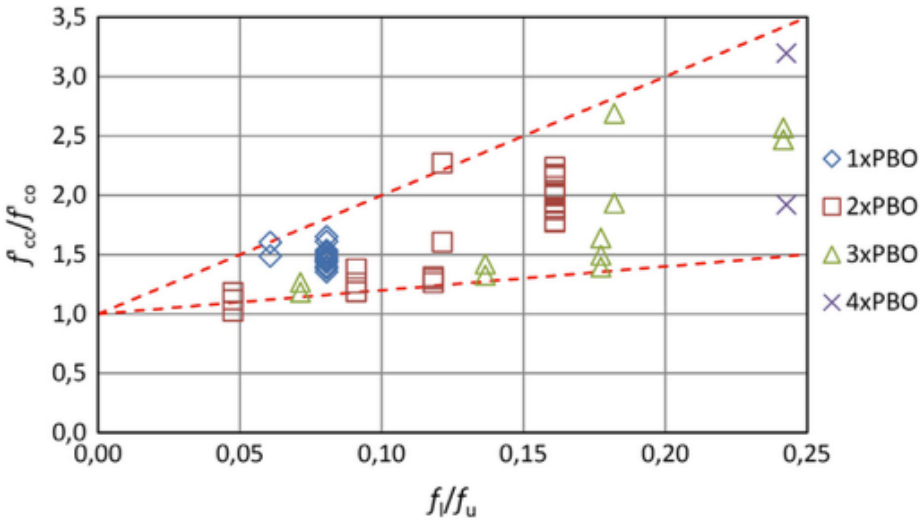

Figure 3. FRCM impact in terms of *fi/fu and fcc/fco* . Taken from *(Trapko, 2014)*

Where:

Fcc is the compressive strength of confined concrete, Mpa.
Fco is the compressive strength of unconfined concrete, Mpa.
F1 is the ultimate lateral confining stress, Mpa.
Fu is the ultimate tensile strength of PBO-FCRM, Mpa.

In addition, since the PBO mesh is a material made of bundles of fibers, which its tensile strength in the lateral direction to the wrapping direction is void and its way of works is totally linear and elastically, the activity of the composite jacket varies closely to the variation of the elastic modulus of the concrete Ec and its transveral deformability ν (Poisson´s rastio). In the figure 4 can be identified clearly the variation of ν once the application of the different PBO layers were performed,

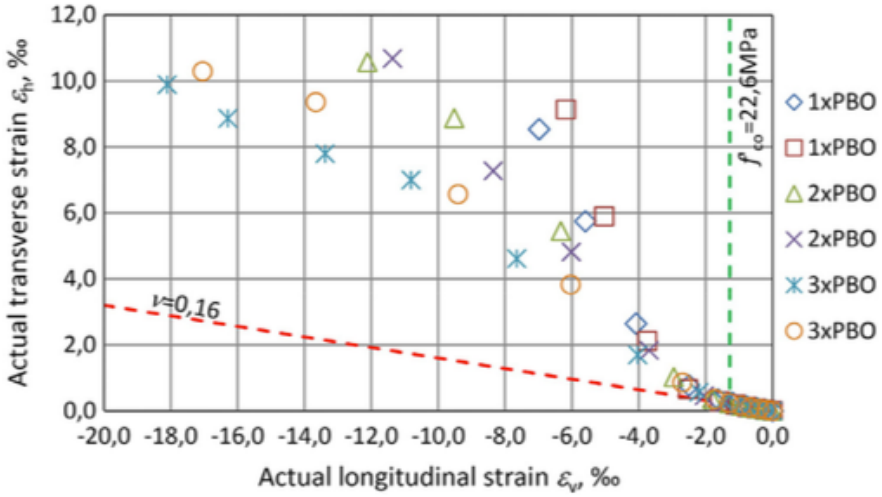

Figure 4 impact of the PBO in terms of strain. Taken from *(Trapko, 2014)*

In addition, is important keeping in mind that within the measurement of the longitudinal and transversal deformation is not being considered the concrete core or the PBO mesh independently, but as a no-homogeneous material made by concrete and the composite. According to the figure 4, where the red dash line is marked as a reference value considering an unconfined concrete core, increasing the number of layers of PBO, the effectiveness of the transverse strengthening is evident, making the specimen capable of higher transversal deformation. Higher transversal deformations than longitudinal were recorded by the author.

Steel

As well as PBO-FRCM, the use of steel fibers embedded within a dry mortar has been studied, representing an important alternative to retrofitting purposes, showing after its application an increase of the flexural strength of the elements intervened. Although the use of this composite materials has shown promising results, the debonding of the composite tends to limit the effectiveness, except in the case where the fibers used have relatively low density, occurring the rupture. (Lesley H. Sneed, 2016).

The experimental campaign carried out by the author consisted in testing 7 specimens using single-lap shear test set-up and five RC beam specimens.

Regarding to the seven specimens tested using shear test set-up, the failure mode was the same experimented using PBO fibers, was due to composite debonding. The behaviour at the failure point was characterized by a brittle detachment at matrix/steel fiber interface and interfacial and surface cracks were observed.

The crack formation starts normally at the loaded end expanding then progressively towards the free end. This phenomenon happens due to the raise of the interfacial shear stresses, having a

relative slip between the internal layers, which is bonded to the concrete substrate, and the external one interacting with the fibers.
On the figure 5 the results obtained by the author are shown, in which the results of the specimens with external matrix layer (DS_K_330_50 series) and without external matrix layer (DS_K_330_50_L) are similar.

Based on the experimental results obtained, it suggests that the initial part of the load response can be approximated as a linear branch corresponding to an elastic behaviour of the bond between the matrix and the fibers (Lesley H. Sneed, 2016). Afterwards, a slight reduction of stiffness is evidenced due to the damage at matrix/fiber interface. Further, the maximum P load is reached increasing the global slip, that can be approximated as a constant until the end with the no distinguished softening phase.

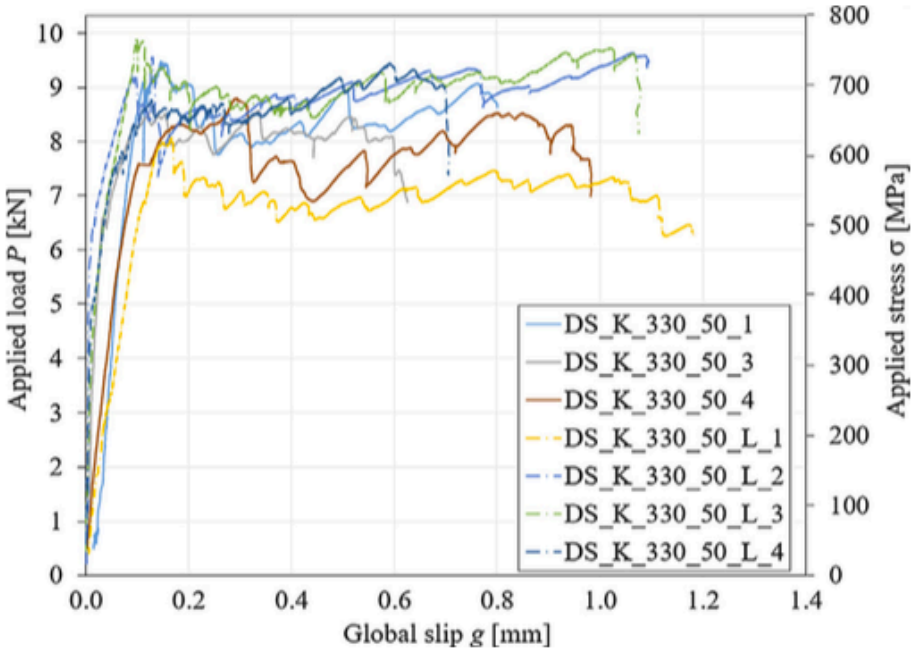

Figure 5 Experimental results. Taken from (Trapko, 2014)

Observing the behaviour obtained by the author, the debonding observed was characterized by a fiber slippage and fracture of the matrix layer at inter matrix/fiber interface (Lesley H. Sneed, 2016).
A post-peak softening response was not observed having a brittle debonding phenomenon, unlike the behaviour observed in different PBO-FRCM composite tests.

1.2. Mechanical Characterization

In order to carry out the structural strengthening, the bonding and mechanical characterization of the materials involved has to be known. This process is implemented through direct tensile and shear bond tests, which its results will define the structural and mechanical parameters to be used towards the strengthening intervention. To guarantee the intended performance of the FRCM system, the bonding behaviour at any interface is of primary importance, influencing in a great manner the final result.

1.2.1. Tensile Test

Factors such specimen production and load application may influence in a great manner the stress-strain behaviour of the tested materials.

A characteristic stress-strain behaviour during a tensile test is shown in the figure 6. The curve can be distinguished as a tri-linear function where: the first zone represents the un-cracked state in which the slope corresponds to the elastic modulus of the matrix. The exceeding of the tensile strength of the matrix is represented in the second zone, where the formation of the cracks starts and the progressive loss of the matrix´s stiffness start occurring. Regarding to the last branch of the curve, the matrix is unable to allow additional cracks and the applied load is sustained only by the fibers.
Having this behaviour, the outstanding parameters to be considered to characterize the tensile behaviour of FRCM, are the stresses and strains at the transitions points and the ultimate stress and strain.

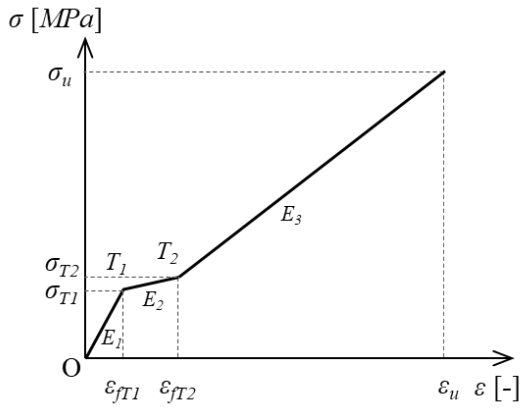

Figure 6. Stress-Strain behavior. Taken from *(Pilla, 2017)*

Regarding to the set-up, the same test can be carried out differently using for instance different clamping methods and measurement methods.

There are two main methods to develop the tensile test and transfer the tensile force to the specimen. The first consist in the direct clamping of the specimen by pneumatic wedges applying a normal force to the plane of the specimen, transmitting in this way the tensile force by friction. The second is called clevis Crip (figure 7), which is the method used for this work, consisting of bonding the metals plates to the specimen ends, which are going to be directed connected to the machine. This clamping method develop a load-bearing behaviour more closely to the field intended conditions.

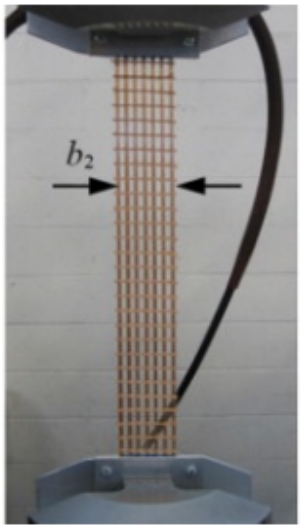

Figure 7 Clamping set up. Taken from *(C. Carloni, 2014)*

Regarding to the geometry of the specimen there are 4 mains shapes to be tested:

- Rectangular shape
- Dumbbell shape (increased section at its ends)
- Bone shape
- V- notched parallelepiped.

Due to the shapes, the first one is the easiest to place thanks to the lack of irregularities. The other geometries can encounter difficulties at the placing stage in the machine, demanding special care.

1.2.2. Shear Bond Test

As well as the mechanical properties of the composite material to be used, the knowledge about the bonding resistance is crucial to the correct characterization in order to predict more precisely the load carrying capacity and the failure mode of FRCM/concrete (Adel Younis, 2018).

Due to the importance regarding to the bonding performance at both FRCM/concrete bond and fabric/matrix interface, several studies have revealed that the most commonly failure occurs at fabric/matrix interface, by means of the fabric slippage within the mortar. The other possible failure modes as can be the fabric rupture or debonding at concrete/matrix interface were rarely occurred.

To test the bonding behaviour at any interface, a certain number of test can be carried out. A single-lap shear test due to its simplicity is commonly performed. The concrete rectangular prism, representing the substrate, is constrained by means of a steel frame and the fabric coming out from the FRCM directed bonded to the prism is pulled out (Figure 8.) (Pilla, 2017). The test is conduced under displacement control.
Nevertheless, the design process regarding to the steel structure acting as a constrain of the substrate can encounter difficulties in terms of eccentricities between the pulling and restraining forces. (Pilla, 2017)

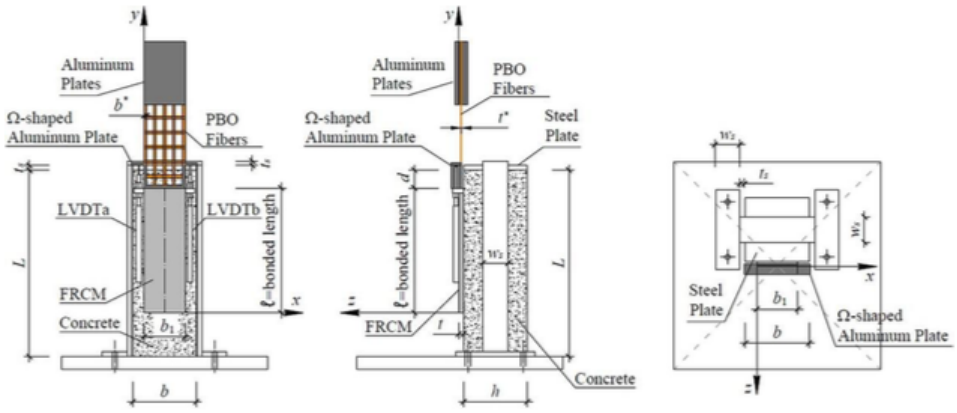

Figure 8. single-lap shear set up. Taken from *(Pilla, 2017)*

On the other hand, the double-lap shear test consists mainly of two rectangular concrete blocks in which FRCM are applied symmetrically. The two fabrics are stretching by the use of a hydraulic jack (Figure 9). A steel plate is placed at the top-end of the fabric between the hydraulic jack and the stretched fabric to guarantee the uniform distribution of the load.

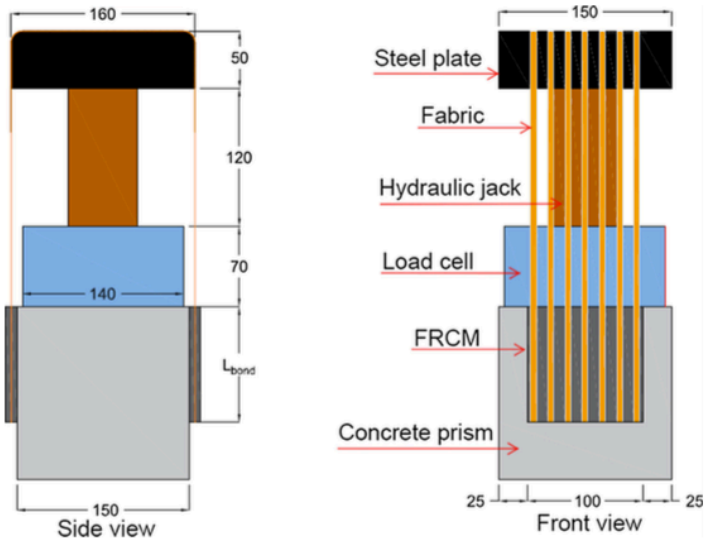

Figure 9 double-lap shear set up. Taken from *(Adel Younis, 2018)*

Finally, depending on the properties of the substrate, the tensile strength of the textile, the textile-matrix bond, the substrate-matrix bond and shear strength of the matrix, different failure modes can be observed during the different tests (Figure 10).

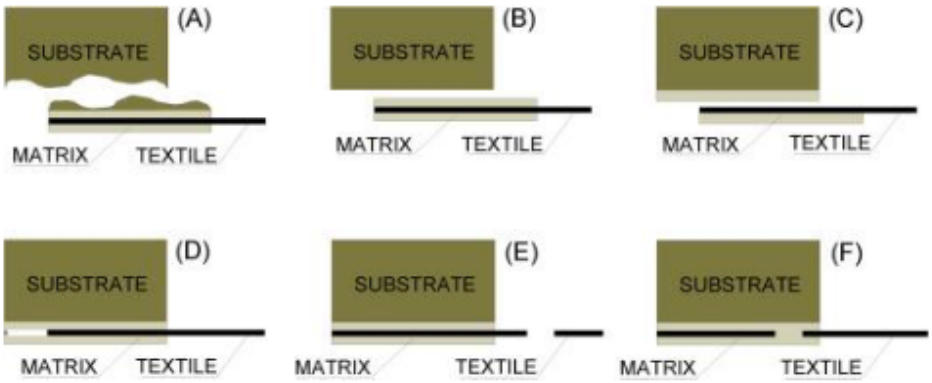

Figure 10 Different failure modes. Taken from *(Pilla, 2017)*

Where:

- The mode A represents the debonding due to a cohesive failure in the substrate
- The mode B represents the debonding at the substrate-composite interface.
- The mode C represents a debonding at fabric-matrix interface.
- The mode D represents a slippage of the matrix within the mortar.
- The mode E represents a rupture of the fabric.
- The mode F represents a rupture of the fabric within the mortar.

1.3. Behavior of Strengthened Concrete Elements

For a correct and precise design of the strengthening technique, is the vital importance the complete understanding of the behaviour of each of the components of the FRP. The bond between the concrete substrate and FRP may play a key role in the final evaluation of the overall structure´s performance and its reliability once the strengthening intervention is carried out.

To characterize the bonding behaviour, many models have been studied and developed, and the stress state may be simulated by means of performing a shear-bond test (Figure 8.) with the FRP lamina externally bonded.

The experimental program heading by Kostiantyn Protchenko, Maria Wlodarczyk and Elzbieta Szmigiera proposes a behaviour analysis of the different solutions to strengthen concrete elements by FRP externally bonded.

During the experimental study, a beam is analysed varying the FRP plate width and thickness as well as varying the plate location, this with the purpose to determine the optimal location where the FRP plate can be placed under the same loads, making possible the measurement of maximum deflection and carrying capacity of each configuration. The set-up is schematized in figure 11 and figure 12.

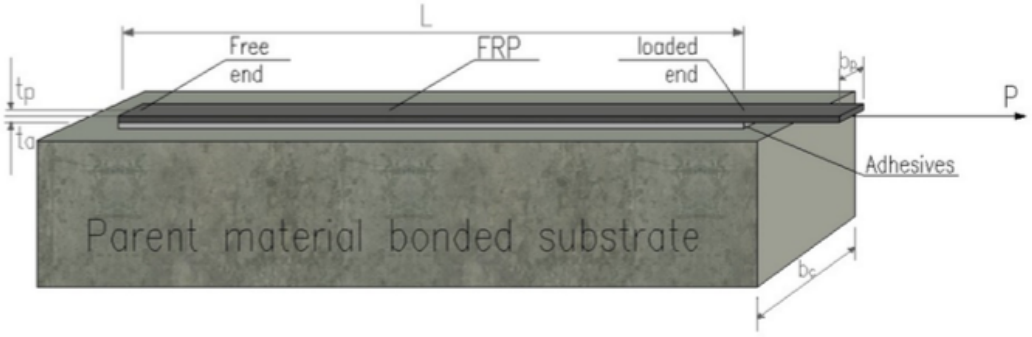

Figure 11 shear-bond test. Taken from *(F. Ceroni)*

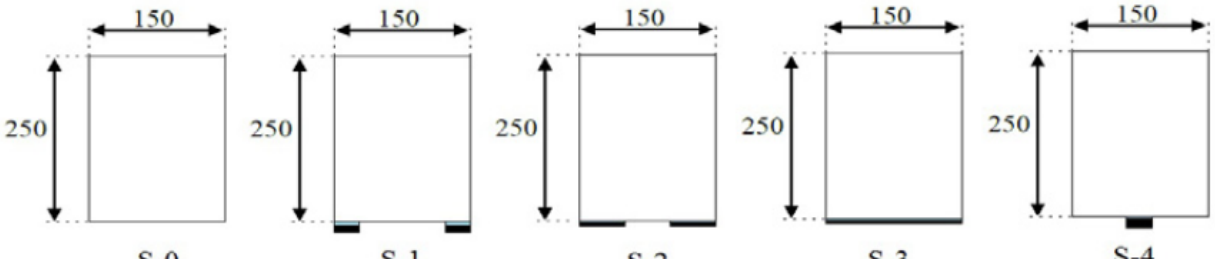

Figure 12 different locations of the FRCM and lengths. Taken from *(F. Ceroni)*

The analysis was performed in LIRA, which is used to finite element analysis. Within the analysis different features as degradability of the glue and thermal load for contraction of the material were considered (Kostiantyn Protchenko, 2015). Among the different results, the best output in terms of maximum load applied and midspan deflection was obtained gluing the plates at the edges of the beam. Despite S-1 was the best configuration according to the results, S-2 and S-4 configuration showed a similar performance, unlike S-3 which its maximum load was considerable lower than the exposed by the rest of configurations.

Besides, due to the recent events which took place in Italy, the high vulnerability of its buildings and its imminent need to implement a retrofit was exposed, showing a typical shear damage in concrete elements (F. Ceroni). Hence, FRCM has gained a special interest during the last decades as an alternative retrofit technique rather than traditional strengthening methods, especially when heritage buildings are involved.
Considering the needs, near to 856 shear bond test results, performed by different researchers, can be collected within the literature. Within the 856 shear bond test results, 347 were related to FRCM applied on a concrete substrate.

Examining the extensive data collected during the recent times, three failure modes were repetitively observed among the different performed tests. Thus, the data obtained was gathered depending upon the failure mode:

- Debonding (include debonding at the mortar/fibers interface and substrate/mortar interface).
- Slippage (refers to movements of the fibers within the mortar).
- Tensile rupture of the fibers. (F. Ceroni)

The distribution of the different failures modes on concrete elements, as it shown in the figure 13, was mainly due to debonding, assuming a main role in the FRCM behaviour as a retrofit intervention.

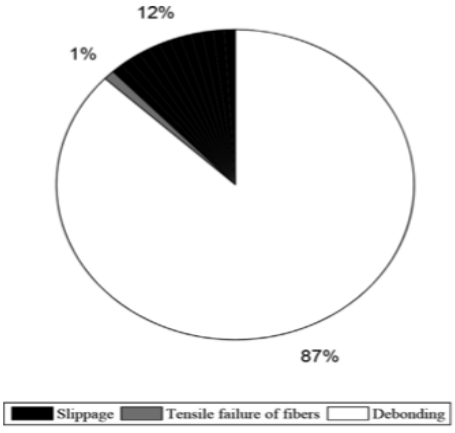

Figure 13 Distribution of different failure modes. Taken from *(F. Ceroni)*

Besides, a poor quality of the mortar can lead to a poor bond strength at mortar/fiber interface, inducing a slippage of the fibers.

Within the data base, a considerable high number of concrete substrates with different strength and different reinforcement strength were tested, reason why the effective length, length greater than the effective one when the debonding load should remain constant without any further increase, [(F. Ceroni)] is different. For the most rigid reinforcements the effective length can be individuated in 150-200 mm, while for the most deformable ones can be in 250-300 mm. (figure 15)

On the other hand, was intended to evaluate the influence of the mortar strength, $f_{c.m}$, on the debonding and slippage failure (figure 14). for both cases the data was highly scattered and clear correlation between the mortar´s quality and the failure mode cannot be determined. The figure of the left refers to the specimens´ failure due to slippage, while the figure on the right refers to debonding failure.

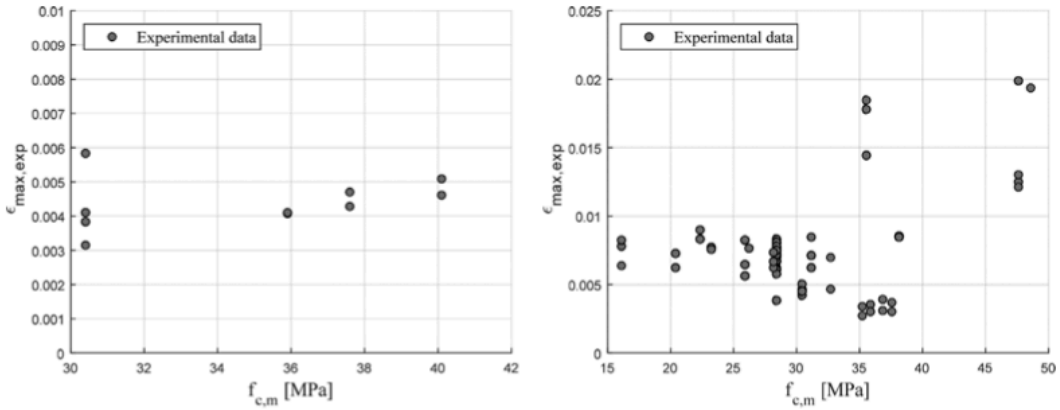

Figure 14 Debonding and slippage failure results. Taken from *(F. Ceroni)*

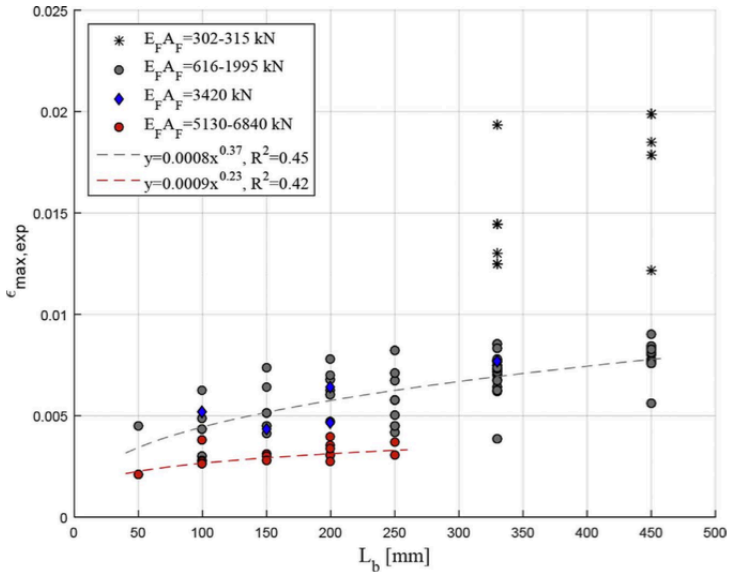

Figure 15 results for different lengths. Taken from *(F. Ceroni)*

Therefore, the outcome provided by F. Ceroni and P. Salzano in their study using the existing data, can be summarized as:

- Deboding was the most common failure.
- There is no a clear correlation between the quality of the mortar and the strain measured of the strengthen concrete substrate.
- In case of debonding, the maximum strain can be increased by means of increasing the mechanical characteristics of the concrete.
- Increasing the rigidity of the FRCM systems, the effective length decreases.

1.4. Design and characterization guidelines

Currently in Europe there is no a guideline or technical specification in which is consigned the corresponding procedure to carry out the different tests and implement the mechanical characterization to implement the strengthening technique to existing buildings through the application of FRCM. Nevertheless, in United States there are some developed codes in which define the design criteria for the reinforcement of the concrete and masonry buildings using FRCM.

The first document is ICC-ES- AC434, developed to provide the necessary guidelines for the evaluation of the FRCM used to carry out strengthening interventions on masonry and concrete buildings. The AC434 establishes requirements for testing and calculations which may lead to the

issuance of a product under research by ICC-ES. (Nanni, 2014). Those reports pass under the evaluation by code officials compiled in the section 104.11.1 of the international building code. The other document regarding to the characterization and implementation of FRCM is ACI 9.4R-13 in which is consigned the history, material properties and recommendations on their use.

Within the AC434 is defined the *material and test methods* and *structural performance test methods*. In these sections the mechanical properties of the materials involved and the recommended tests to characterize the system (tensile test, orthogonal bond test and durability resistance) are described, respectively.

On the other hand, within the ACI 9.4R-13 is described the general considerations for the reinforce procedure to perform on masonry and concrete buildings.

In Italy, currently the guideline is still in process, in which the results and different experimental campaigns heading by different researchers are being studied aiming to the standardization of the use of FRCM as a reinforce technique along the territory.

1.5. Scope of the thesis

The main objective of the present job is the study and the understanding of the bonding behavior on FRCMs. To carry it out, an experimental campaign was developed where parameters such the way of casting were considered, being some FRCMs casted from the top of the specimens and others from the bottom. The material used for the substrates was concrete.
Besides, an important part of the thesis is dedicated to the study of the load distribution among the bundles within the textile, evaluating as well its impact in terms of ultimate strength.
In the last part of the job, the discussion of the results was developed, where the parameters considered are evaluated, obtaining the corresponding outcome.
Currently in Europe there is no a specific guideline which can be followed, and the academic material is very limited, reason why this thesis is looking forward to stablish some basic considerations for the future jobs, providing experimental data and its corresponding analysis.

2. EXPERIMENTAL TESTS.

2.1. Introduction.

Fiber Reinforced Cementitious Matrix (FRCM) during the last decades has gained special attention within the engineering field, due to its wide application for retrofitting purposes. However, as well as its wide applicability, its behaviour is extremely complex due mainly to the heterogeneity of the constitutive materials. The interaction between the fibers embedded and the matrix, having both a different mechanical behaviour, can lead to different failure modes, which should be analysed and evaluated for each specific case.

During the study of the FRCM behaviour for its further implementation, researches have idealized is behaviour as a tri-linear behaviour. In the first phase the behaviour observed can be described as an elastic performance, depending in the major part upon the matrix properties. The second phase is governed by the cracks-initiation phenomenon and its propagation and finally in the third phase the matrix is completely cracked and the applied load in supported only by the textile.

During the experimental tests, was evident that the impregnation and behaviour of the embedded textile within the matrix was different for the different specimens tested. Hence, the overall tensile strength achieved for the different cases was naturally different.
Twelve concrete specimens were tested, in which six the fiber used to carry out the strengthening was PBO, and the others six were steel. The experimental data can lead to some recommendations for the further application on field.
An important and substantial feature of the set-up is the bond behaviour at the different interfaces, feature which governs in a great manner the overall performance. Reason why the well understanding of the interfacial behaviour has a special impact on the final result. Hence, the mortar capability to penetrate the grid can lead to better results.

On the other hand, is important to highlight the different procedures to measure the deformation, some more precise than others. Nowadays there are a great variety and methods to asses this variable. The use, for instance, of strain gauges can lead to an accurate local information, but is inadequate in the specific case of multi cracking behaviour. The use of extensometers is reliable in terms of alignment and avoid possible out of plane bending moment. A very precise set-up providing accurate information include LVDTs place on opposite sides of the specimens. On the other hand, a photogrammetry is an innovative method, which can provide a more precise information in terms of load distribution among the different bundles of the textile (Carozzi, 2016). For the present job, the tools used to perform the distinct analyses were LVDTs and photogrammetry.

2.2. FRCM materials characterization

The analysed system consisted in a PBO and steel fiber embedded in a mortar. The mortar used for the different tests was the same, making possible the comparison among the PBO and steel results. The six PBO textiles have the same features as well as the six steel textiles, however, the way how they were applied on the concrete prisms was different, being some of them cast from top and the others from bottom of the specimens.
For the mechanical characterization of the twelve different specimens, the image correlation (IC) method was used, comparing the results obtained with the results obtained using a conventional method.

2.2.1. (P, 2013) (Hadigheh SA, 2015) (Ascione L, 2015) (Pellegrino C, 2013)PBO

The nominal width *b* and average thickness *t* of one longitudinal fiber bundle were 5 and 0.0092 mm, respectively. The *t* defined in this job differs from the equivalent thickness provided by the manufacturer. The equivalent thickness provided by the manufacturer assumes that the fibers are spread evenly over the entire width of the composite instead of bundled. Hence, the *t* used for the present job represents the thickness of the fiber bundled, having a cross section of with *b.* (C. Carloni, 2014)

2.2.2. Steel.

On the following table are presented the mechanical properties provided by the manufacturer,

Property	**Low density**
Number of cords/mm	0.157
Tensile Strength [Mpa]	>3000
Elastic Modulus [Gpa]	>190
Break Deformation [%]	>2
Equivalent thickness [mm]	0.084

Table 2 Mechanical properties of the steel fibers

2.3. Behavior of the FRCM materials under tension.

In the following section the behaviour of the FRCM materials under a tension load application is studied, analysing the influence of different parameters as the way how the specimens were cast.

A comparison between the different results between PBO and steel is reported as well as the results obtained among the six PBO reinforced specimens and six steel reinforced specimens.

2.3.1. Mechanical performance of FRCM (PBO) under tension.

For the purpose of the present job, the strengthening techniques were carried out using PBO-FRCM and STEEL-FRCM, having both different mechanical properties and applicability fields. The results exposed by (Trapko, 2014) have shown that the PBO-FRCM system turned out to be an effective method to increase the bearing capacity of compressed concrete elements through the confinement using PBO-FRCM systems. This method raises its efficiency as lower the concrete class is, having the strengthening technique a more overall significant impact. Due to its impact on low-concrete class, its applicability on weak constructions (old construction) has a considerable effect on its ultimate capacity. But still the main parameter to be considered and evaluated regarding to the use of FRCM is the bond behaviour at all the interfaces.

Finally, the tests performed to the six different specimens were carried out implementing the same clamping method, showed in the figure 16 consisting in a steel plates glued to the free end of the fibers. Therefore, the main load transfer mechanism between the clamping and the specimen is adhesion tension and shear, avoiding with this the slip phenomena that may occur between the clamping and the specimen.

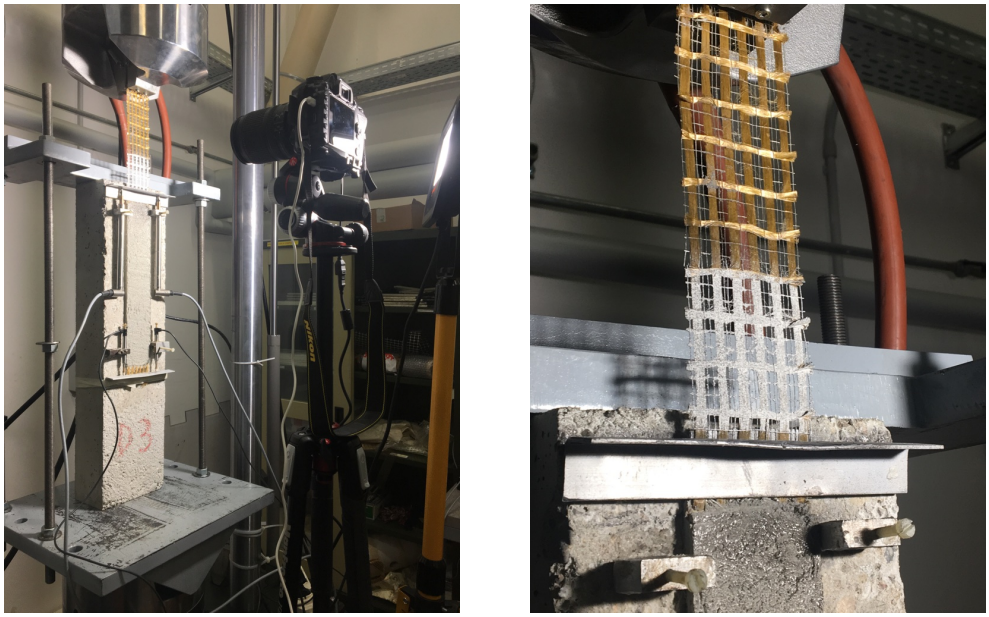

a) B)

Figure 16 a,b) debonding test set up

Four LDVTs were placed along the FRCM, two at the loaded end and two at the bottom, registering with this the overall displacement experimenting by the textile at its two ends during the test execution. The LVDT was momentaneously glued at both ends using a steel plate fixed to the specimen (figure 16).

2.3.1.1. Results

In the following section, the results obtained during the test execution for the six different specimens are presented, in which the overall displacement is registered. The displacement showed corresponds to the loaded and free end measured by the use of LVDTs.

Initially, one of the assumptions and hypothesis to corroborate was the load distribution among the bundles before the debonding phenomenon start occurring, reason why the use of LVDTs at different locations along the specimen was required, to register the possible rotation of the textile in case where the load distribution start becoming non-uniform.

The nomenclature used to distinguish the different specimens is DS_300_60_X, where 300 represents the length of the specimen in millimetres, while 60 represents the width and X refers to the specimen´s number.

Referring to the four LVDTs used at top and bottom, their measures are discretized using the nomenclature showed in the figure 17.

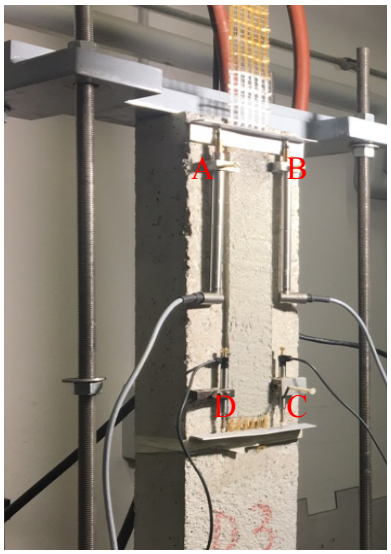

Figure 17 positioning of the LVDTs

- DS_300_60_1

The blue line describes the measures registered by the LVDTs placed on the loaded end (top part of the specimen) corresponding to the A and B points highlighted on the picture, while the green line represents the displacement experimented at the free end of the textile, C and D points.

Initially only the loaded end is supporting completely the load and when the debonding start occurring, the free end start to support partially the load, hence, start its displacement.

As it was explained before, four LVDTs were used in total, using two at the top and two at the bottom. The blue line in this case represents the average of the displacement measured by the two LVDTs on the top, and the green line the average measure at the bottom (figure 18).
It is worth to highlight that once the peak load is reached, the PBO fiber starts its softening phase, exposing with it its ductile behaviour.

Additionally, the individual data corresponding to each of the LVDTs was plotted (figure 19) observing the difference among them. This difference lead to the non-uniform load transfer assumption. On the top part, the LVDTs lectures are different, having a higher displacement the right part of the textile before debonding (B higher than A). The same behaviour was observed on the bottom part, assuring that the transmission of the load within the textile is non-uniform, being some bundles supporting a higher part of the load than others.

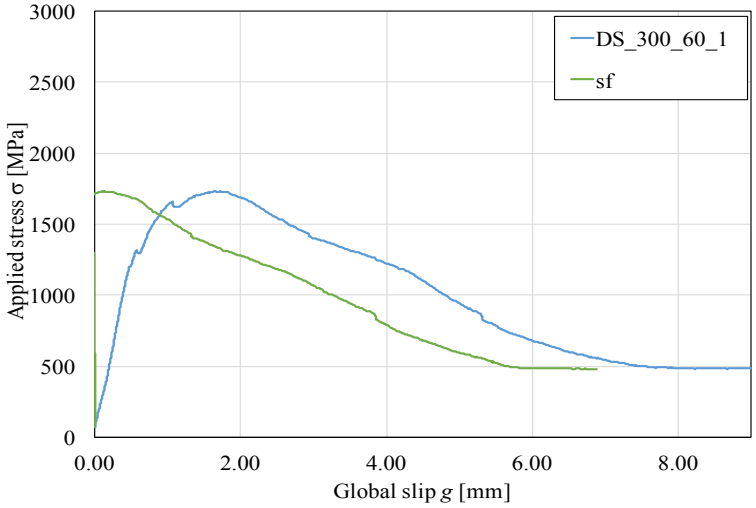

Figure 18 Stress-Slip results (loaded and free end)

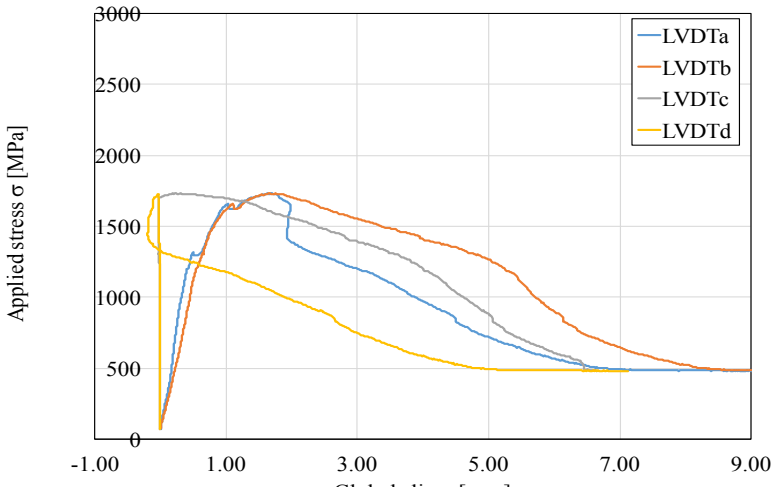

Figure 19 Stress-Slip results of the four LVDTs

Some LVDT data, specifically the one corresponding to the bottom part (C and D), have at certain point negative values, and it is due to the reference plane and the way how the LVDTs were placed. Despite the negative values observed along the C and D line, their trend is the same observed along the A and B, where the displacement registered for both was not equal.

- DS_300_60_2

The methodology used for the execution of the test of the first specimen was the same used for the present one, observing and evidencing the behaviour mentioned previously, where the load initially is fully supported by the top end, and near to the peak load, a displacement at the bottom start to be slightly present due to the debonding initiation.

Regarding to the behaviour reported in the figure 20, the differentiation among the displacement lectures are evident, exposing the same behaviour present in the first test.

Although the materials used and the set up implemented for the tests were exactly equal, the peak load, for instance, was slightly different.

The main parameter which can affect the maximum strength reached by different specimens is the bonding interaction at matrix/textile interface depending mainly upon the impregnation grade of the matrix within the textile.

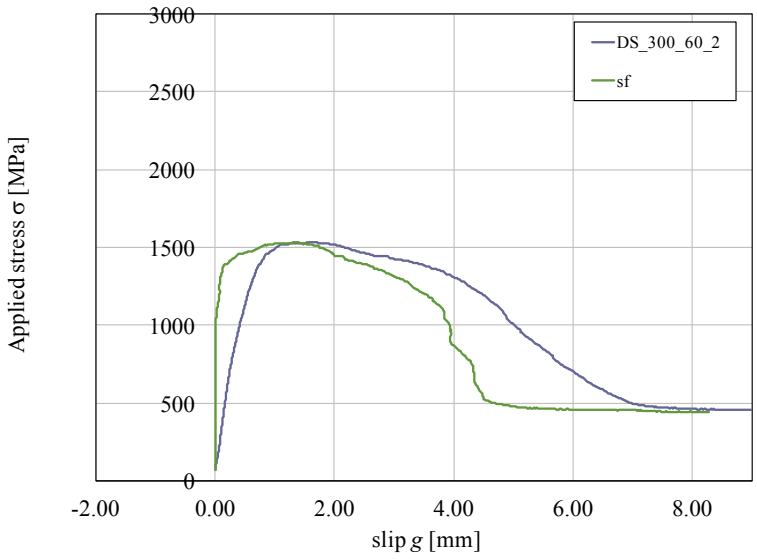

Figure 20 Stress-Slip results (loaded and free end)

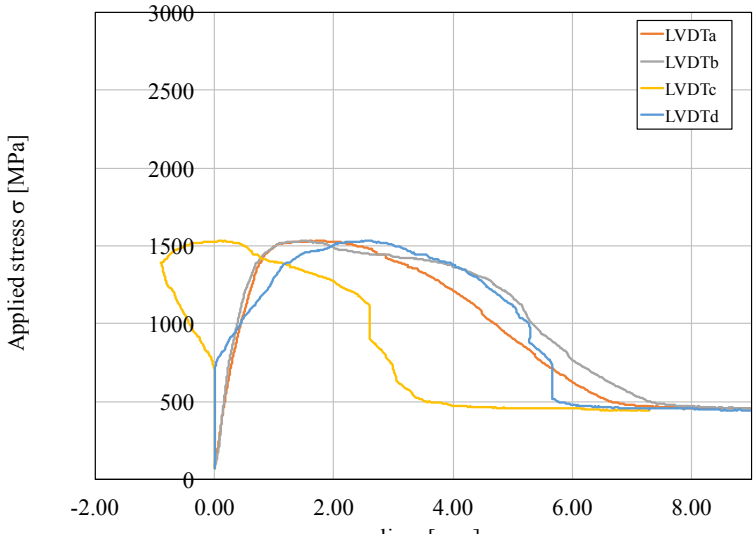

Figure 21 Stress-Slip results of the four LVDTs

- DS_300_60_3

As it was reported before, the tendency of the displacements at top and bottom is the same, differing in the maximum strength reached. The behaviour reported regarding to the bottom (figure 23) was the same evidenced during the execution of the second specimen, in which the LVDT at the position C at certain point start assuming negative values for a specific interval of time due to its reference axis, representing the differentiation, in terms of displacement, experimented at the bottom of the specimen, leading to a vaguely rotation.

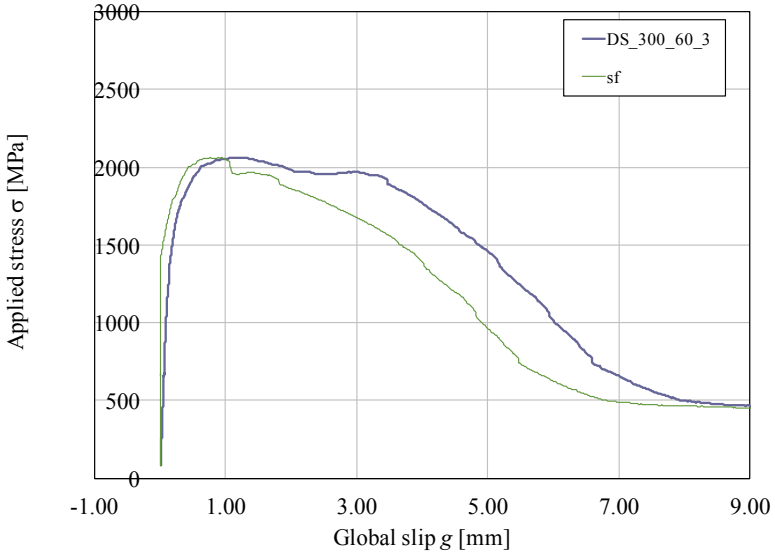

Figure 22 Stress-Slip results (loaded and free end)

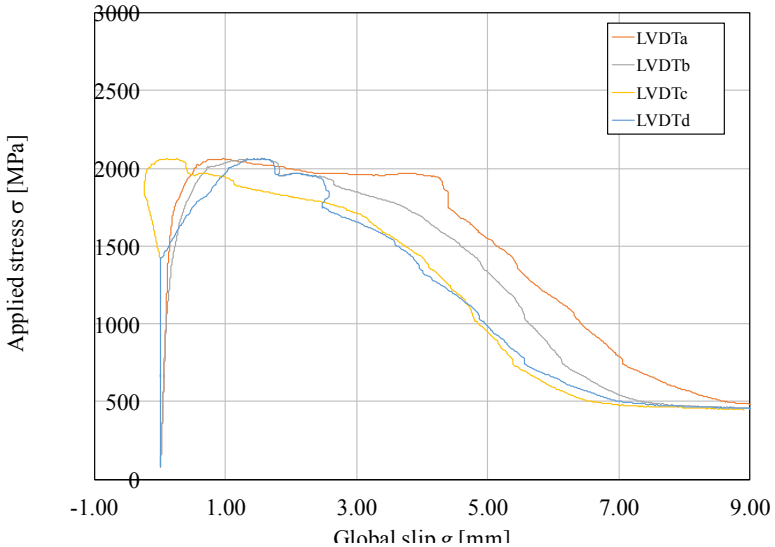

Figure 23 Stress-Slip results of the four LVDTs

- DS_300_60_4

In terms of shape and trend of the line, no changes are reported within the graphs, the factor which is changing continuously is the peak load reached by the different specimens, and in some cases the variation can be significant. The fourth specimen reached 1200 Mpa, while the third and first one were about 2000 Mpa. The variations evidenced, as it was mentioned before, are due to mainly the impregnation level of the matrix within the textile.

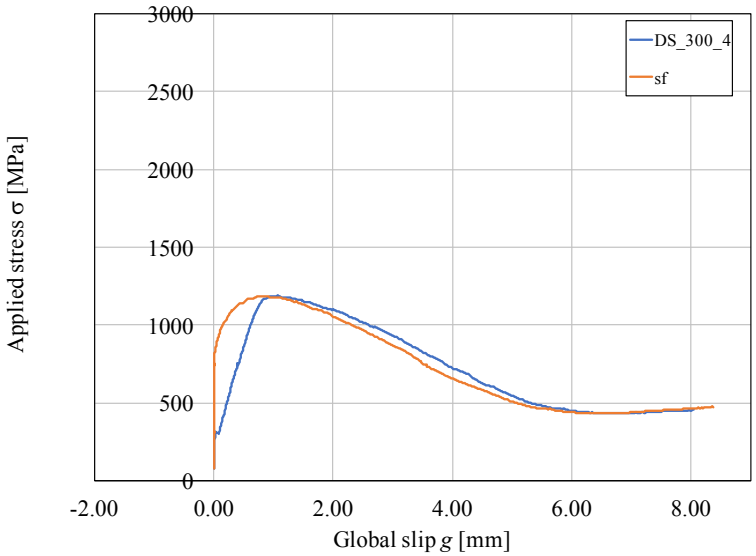

Figure 24 Stress-Slip results (loaded and free end)

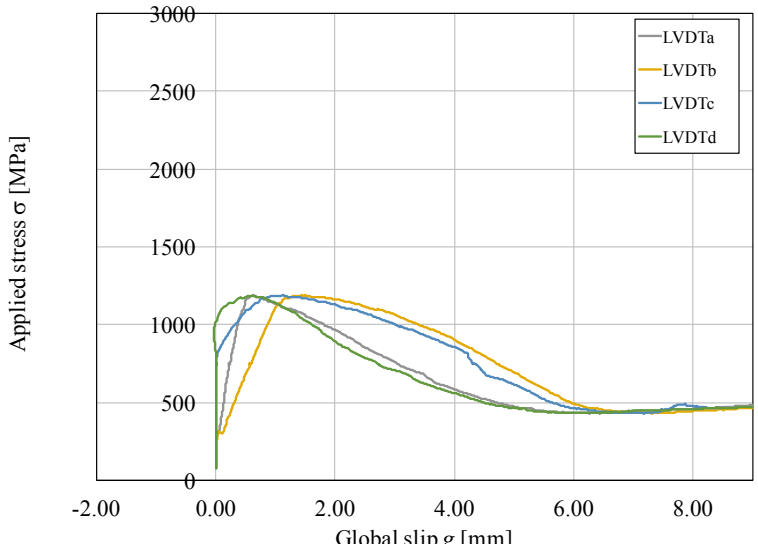

Figure 25 Stress-Slip results of the four LVDTs

- DS_300_60_5

As it was expected, the behaviour kept the tendency registered for the specimens tested before, corroborating the behaviour reported in the literature. Although the trend is equal, once again the peak load reached varies from specimen to specimen, in some cases, considerably.

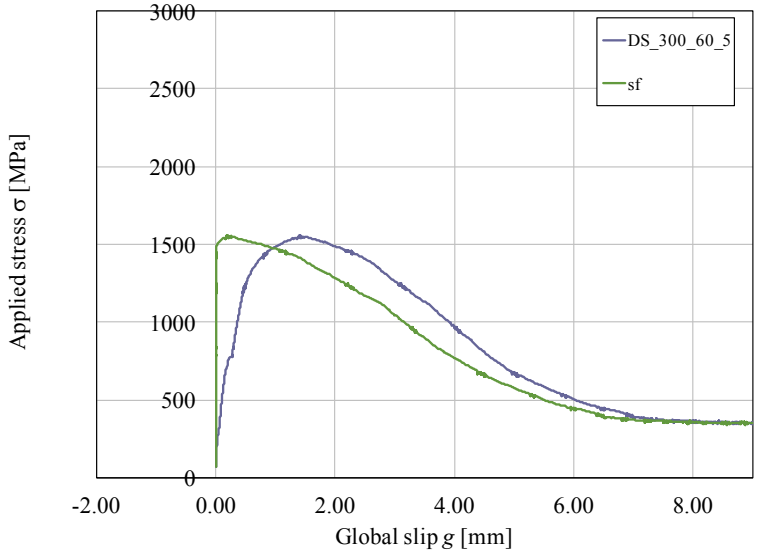

Figure 26 Stress-Slip results (loaded and free end)

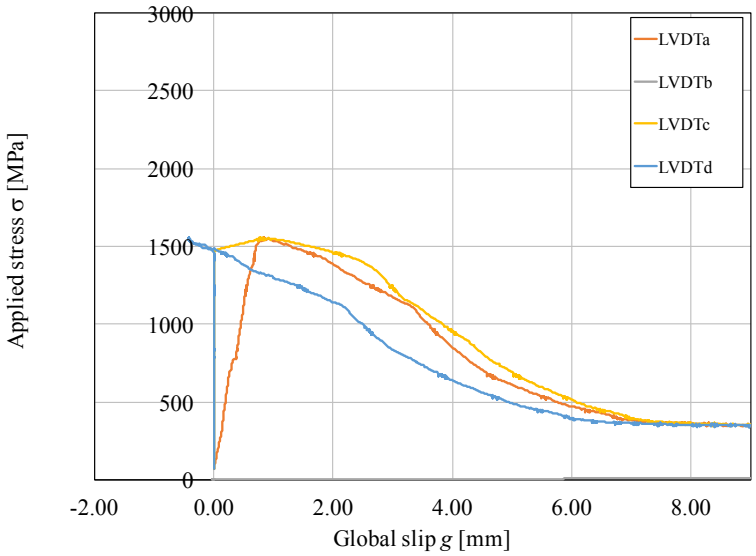

Figure 27 Stress-Slip results of the four LVDTs

- DS_300_60_6

Finally, the six specimens were tested, observing in each one of them the trend expected according to the behaviour consigned on the research data. Observing the same behaviour among the different specimens, the further analysis should be addressed to encounter the cause why the peak load for the different specimen can vary, in some cases, in a considerable way, being an issue to standardize the procedure regarding to the execution of the test and in the manufacture process.

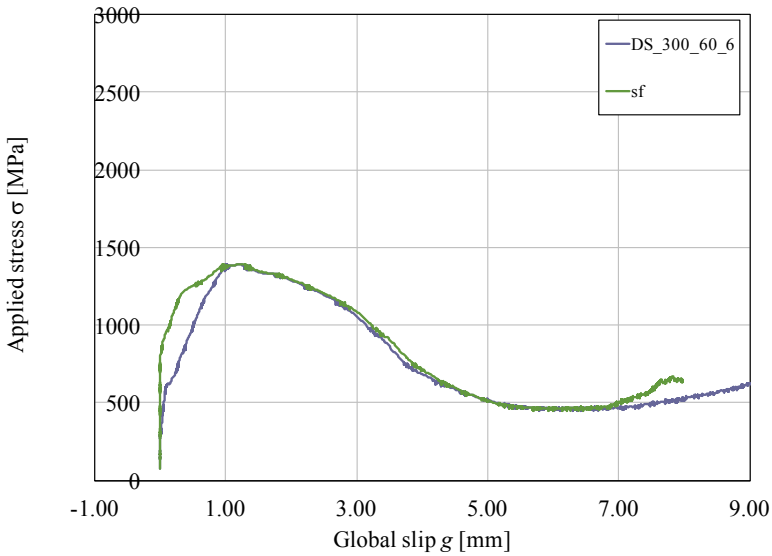

Figure 28 Stress-Slip results (loaded and free end)

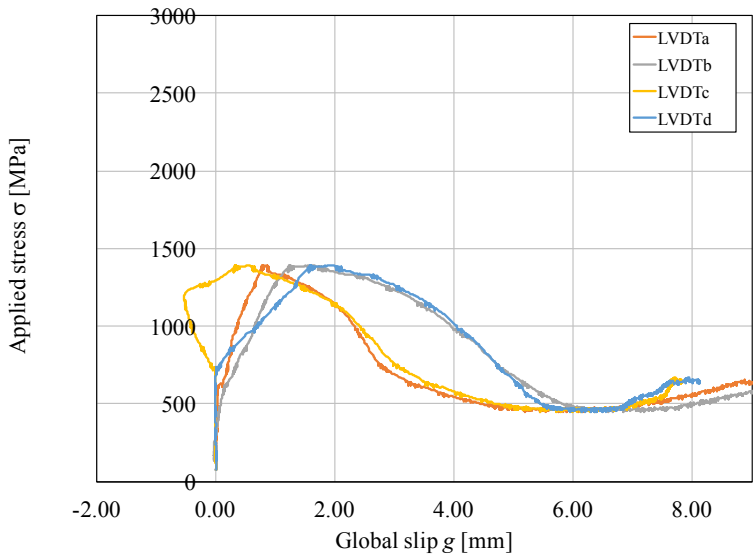

Figure 29 Stress-Slip results of the four LVDTs

Concluding, in the figure 31 is shown the 6 results related to the FRCM using PBO, in which is possible to appreciate the influence of certain parameters in the final performance. The parameter for the present job is the way of casting. The casting procedure for some specimens was carried out from the top of the concrete prism, and for the other was realized from the bottom.

Additionally, one of the initial assumptions was the non-uniform load distribution among the different bundles of the textile, which means the stress that each bundle was subjected to was different respect each other, resulting in a differentiation in terms of displacement. This is strongly observed in the figure 30, where the LVDTs at the top of the specimen (A and B) registered a different displacement between them as well as the LVDTs at the bottom (C and D). According to the figure 30, on the top of the specimen the displacement registered at A is higher than the one registered at B. The behaviour observed at the bottom was similar, being the displacement at D higher than the displacement registered at C, resulting in a slight rotation. Hence, the initial assumption was proved and was strongly noticed that the load transmission among the different bundles was not uniform. However, the use of LVDTs, in terms of load distribution in the different zones of the textile used, at certain point start encountering some limitations. Nevertheless, is evident that with the current set-up is possible to observed the non-uniform load distribution, but is not well known what specifically is the stress that each bundle is subjected to, and how the total load is distributed, in this case, among the six different yarns. Therefore, was necessary to carry out a photogrammetry analysis, which is going to be shown in the following sections.

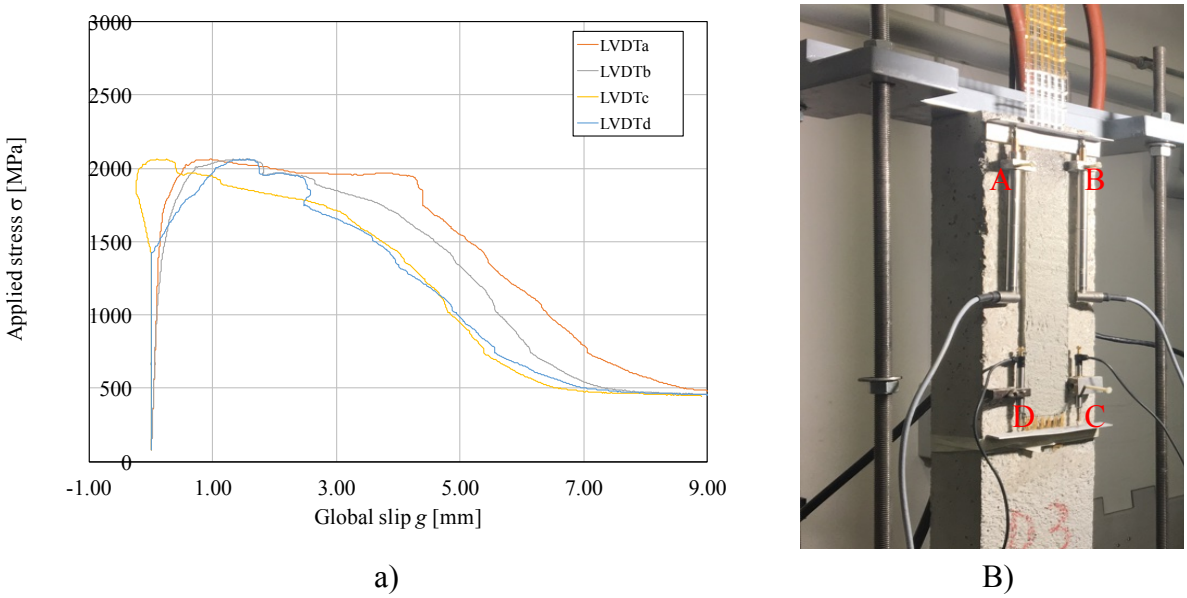

Figure 30 a) Stress-Slip results of the four LVDTs; b) nomenclature for the LVDTs position

In the table 2 the values of the ultimate stress of each specimen and its average are reported. The dash lines represent the specimens cast from top and the continuous the specimens cast from bottom. Therefore, is evident in this case that the way of casting does not influence significantly on the specimen´s performance, being dash and continuous lines mixed and not well differentiated within a specific range.

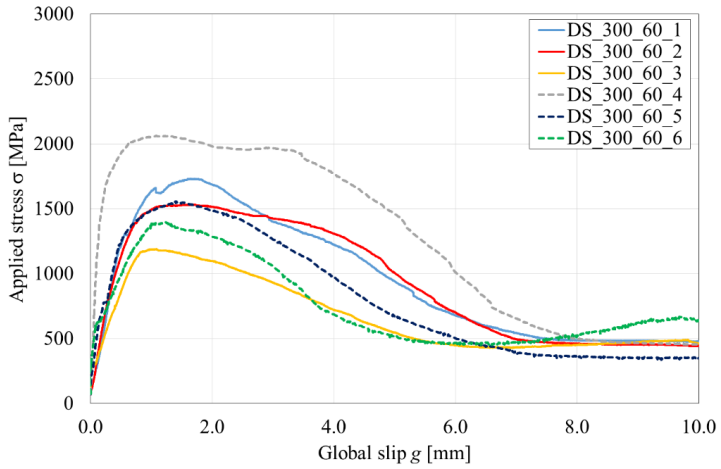

Figure 31 overall results of the six specimens

	σ_{max} [MPa]	Avg σ_{max} [MPa]	CoV
DS_300_60_1	1732		
DS_300_60_2	1533	1485	18.46%
DS_300_60_3	1190		
DS_300_60_4	2063		
DS_300_60_5	1556	1671	20.85%
DS_300_60_6	1395		

Table 3 Results in terms of ultimate strength

In the table 3 is reported the ultimate strength and strain related to the concrete specimens strengthened with the FRCM using PBO. The value *n* refers to the number of bundles which the textile contains. The materials and parameters used for these six tested specimens were the same except for the way how the FRCM was applied on the prisms.

The variation among the ultimate strength values is due mainly to the interaction at textile/mortar interface, where the bonding and permeation reached by the mortar within the textile will dominate the final performance.

Additionally, as it was expected, once the maximum strength was achieved, when the debonding occurs, the slippage phenomena initiates and the movement at the free end of the textile starts (figure 32). This behaviour, which is represented by the green line, shows the global slippage at the free end of the textile, tendency clearly noticed during the other five tests as well.

Type	Name	n	Strength [MPa]	ε max
PBO	DS_300_60_1	6	1732	0.008407891
	DS_300_60_2	6	1533	0.007443406
	DS_300_60_3	6	1190	0.005777253
	DS_300_60_4	6	2063	0.010013879
	DS_300_60_5	6	1556	0.0075522
	DS_300_60_6	6	1395	0.00677238

Table 4 results in terms of ultimate strength and strain

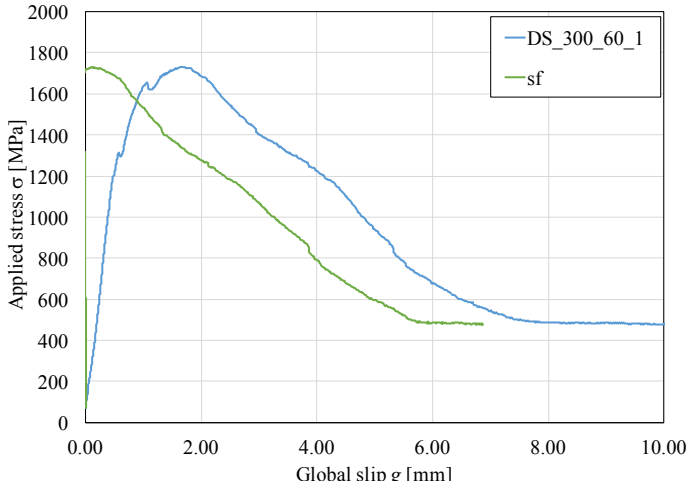

Figure 32 General behavior of PBO-FRCM

Within the different parameters that can affect the final performance and the variation on the ultimate strength as it is noticed in the figure 31, the measures taken when FRCM material was placed on the concrete prisms can influence in a great manner as well as the different grade of permeation of the mortar into the textile. Hence, the equipment and personal responsible to carry out this activity may affect the final performance, leading to different results.

As a common behaviour observed during the test execution of the five specimens was the softening phase once the peak load is reached due to the debonding phenomenon. As it will be observed further, that this behaviour was not observed within the steel performance tests, in which the failure mode once the peak load is reached occurs abruptly.

2.3.2. Mechanical performance of FRCM (steel) under tension.

The procedure followed during the testing process of the PBO fibers was the same followed for the steel fibers. Six concrete prisms were placed and the free end of the fiber were glue to a steel plate, generating only tension and shear stress avoiding any slippage phenomena within the plates during the load application. As it can be noticed on the figure 33, four LVDTs were placed, two at the bottom part and two at the top one, making possible the measurement of the corresponding displacement.

On the following section the results obtained regarding to the steel-FRCM are presented, pointing out the main differences observed in comparison with the overall performance obtained using PBO-FRCM.

a) b)

Figure 33 a,b) set-up for steel-FRCM

2.3.2.1. Results

As it was presented in the previous section, the stress-strain relation of the specimens tested are presented considering both the global slippage resulting from the average of the measures registered by the LVDTS at top and bottom and the individual displacement of each LVDT. Following the trend observed in PBO-FRCM, the load distribution among, in this case, the eight bundles was not equal, being some of the yarns subjected to a higher stress.

The nomenclature used to differentiate the specimens is denoted by DS_S300_60_X, where 300 and 60 are the length and width of the specimen in millimetres respectively, while the X refers to the specimen number.

- DS_S300_60_1

For the case of the steel, as it is showed in the figure 34, the displacement registered at the bottom of the fibers was negligible. The load was not transmitted to the bottom part of the textile until the very end of the test execution when the debonding start occurring. Hence, the lectures of the LVDTs located at the bottom were nearly nil.

Unlike PBO fibers, the behaviour of the steel was not ductile, reaching its failure in a sudden mode when the debonding phenomenon takes place at matrix/textile interface.

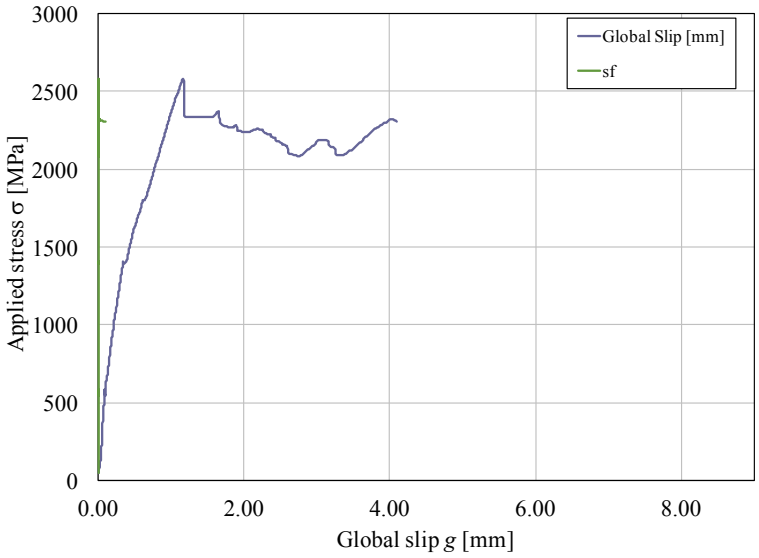

Figure 34 Stress-Slip results (loaded and free end)

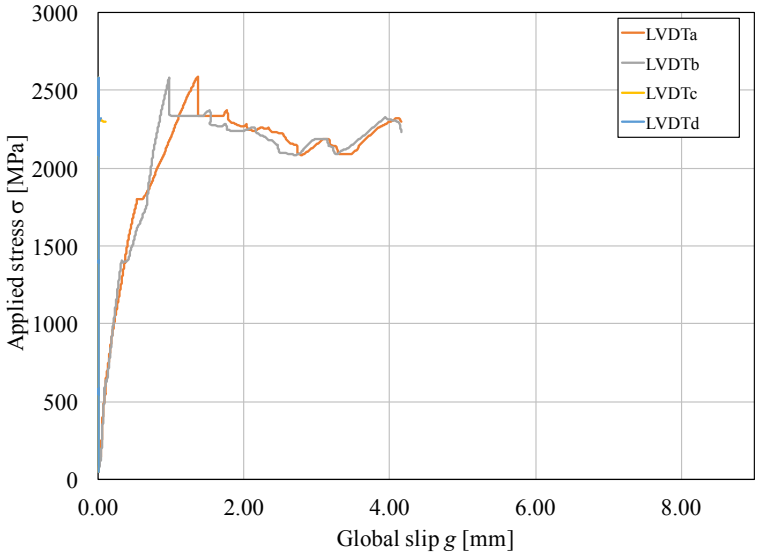

Figure 35 Stress-Slip results of the four LVDTs

- DS_S300_60_2

For the case of steel, the variation in terms of peak load was not scatter as it was noticed during the PBO tests execution, in which sometimes the variation can be up 30%. The trend followed within the steel results is equal, where the bottom part does not register a significant displacement.

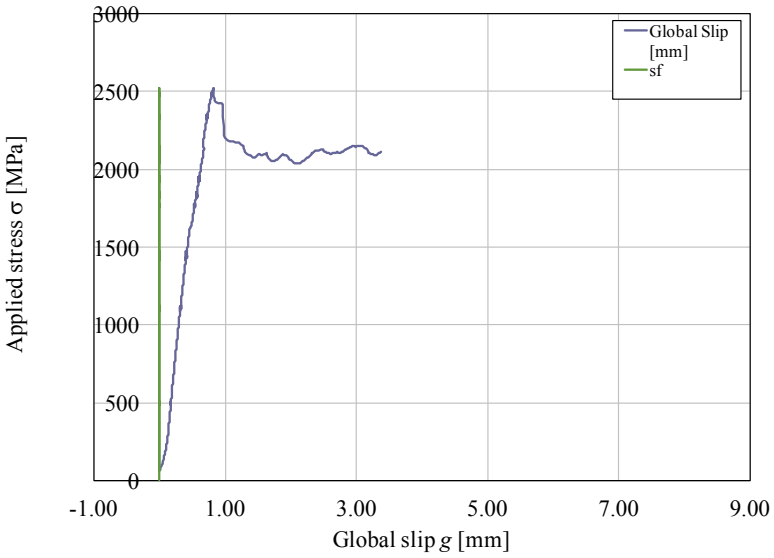

Figure 36 Stress-Slip results (loaded and free end)

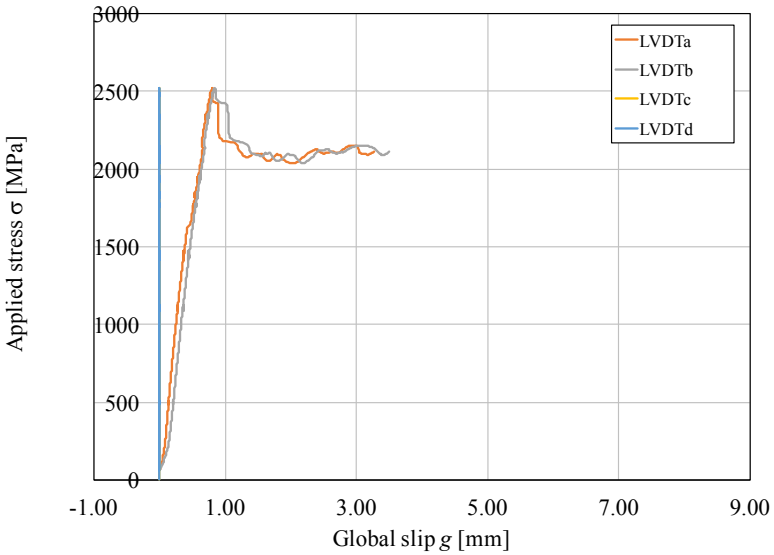

Figure 37 Stress-Slip results of the four LVDTs

- DS_S300_60_3

the pattern evidenced in the previous specimens is presented, even in the peak load reached during the test, which although the variation does exist, it is not substantial. The displacement

registered at the bottom of the textile was practically nil, being the top part of the specimen subjected to the load application until debonding start to be present.

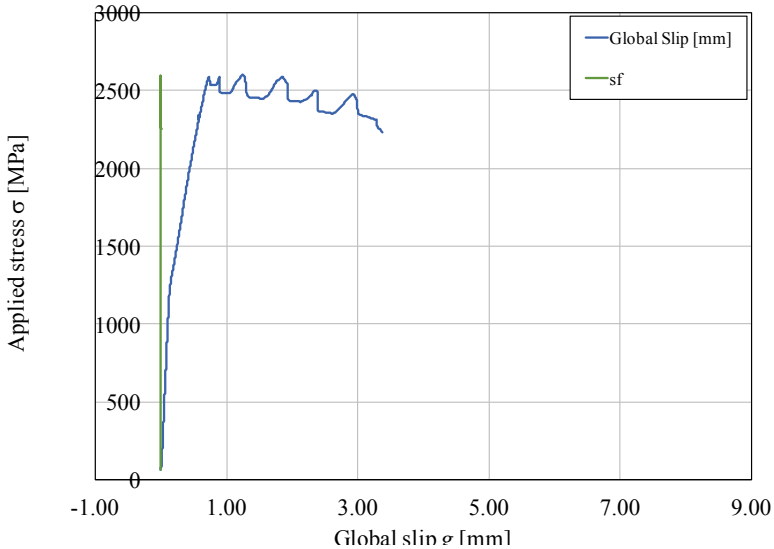

Figure 38 Stress-Slip results (loaded and free end)

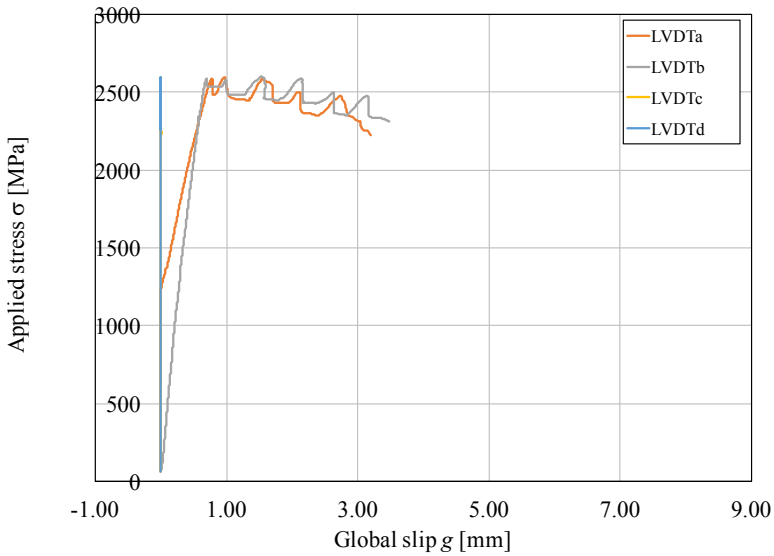

Figure 39 Stress-Slip results of the four LVDTs

- DS_S300_60_4

The behaviour registered does not present any variation comparing to the previous specimens.

Following the tendency, at the bottom of the textile there was not a substantial displacement registered.

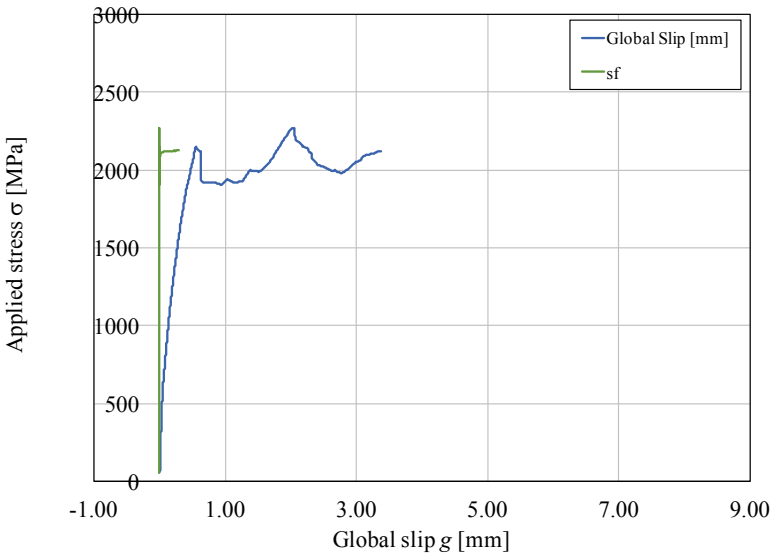

Figure 40 Stress-Slip results (loaded and free end)

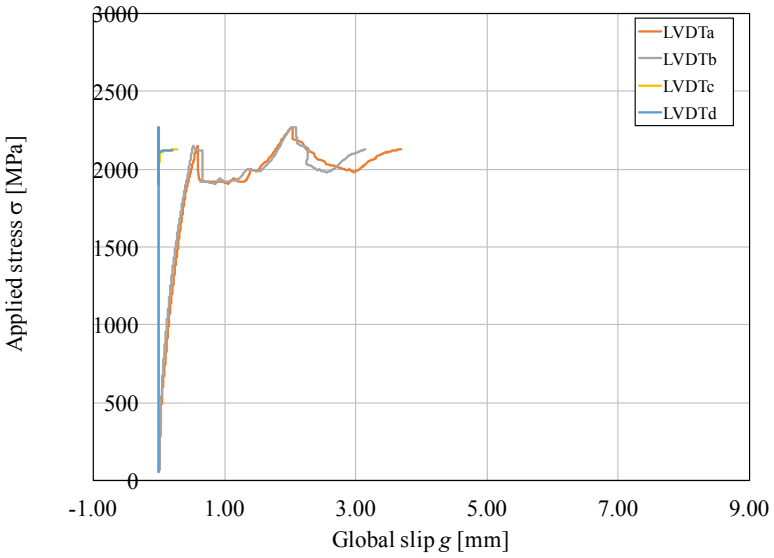

Figure 41 Stress-Slip results of the four LVDTs

- DS_S300_5

Observing the different curves and its corresponding comparison among them, unlike PBO fibers, the distribution among the different steel bundles was considerable more uniform, having similar displacements the top part.

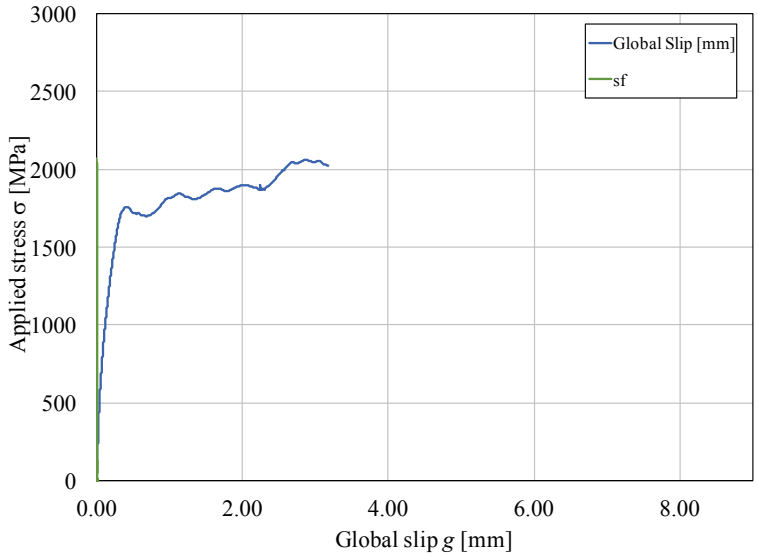

Figure 42 Stress-Slip results (loaded and free end)

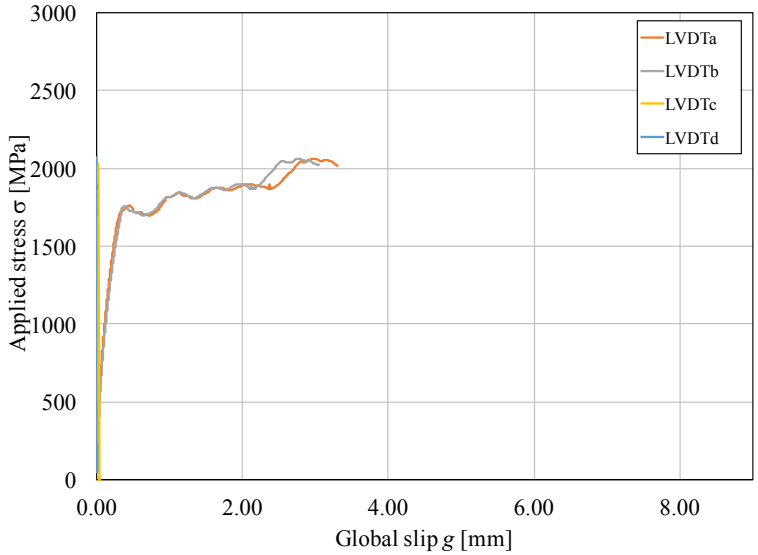

Figure 43 Stress-Slip results of the four LVDTs

- DS_S300_60_6

The trend observed during the execution of steel-FRCM composite was in way more regular that the performance observed during the testing season of PBO-FRCM composites. In this case the way how the specimens were casted has a more notorious impact on the overall performance of the specimens. The final result comparison is presented ahead.

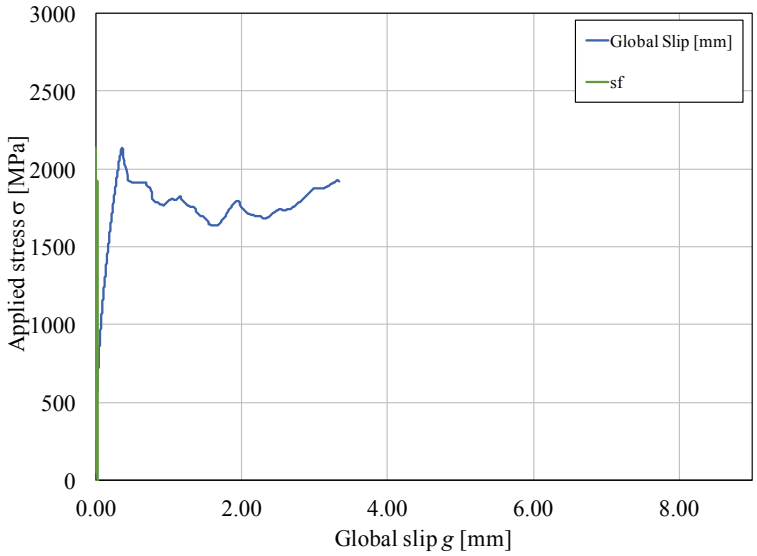

Figure 44 Stress-Slip results (loaded and free end)

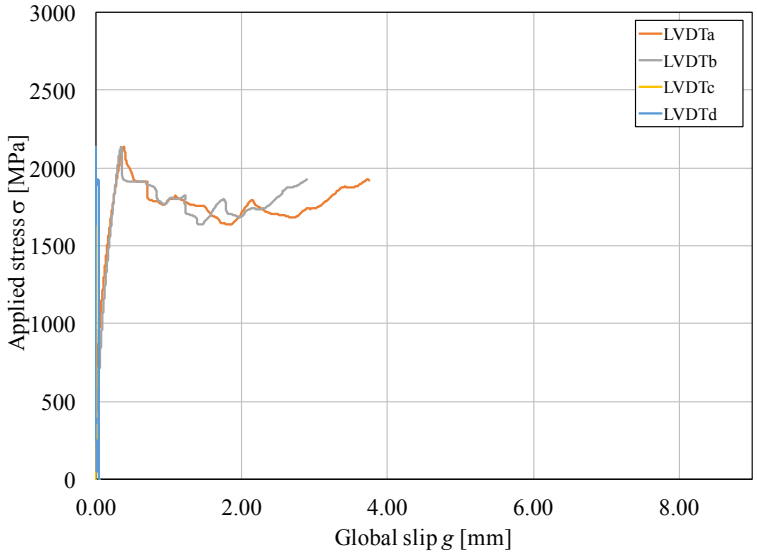

Figure 45 Stress-Slip results of the four LVDTs

For the case of the steel fibers, the casting process was carried out in a different way for the three specimens, being casted from the top and the other three from the bottom.

Additionally, the behaviour expected initially in terms of load distribution was the same as it happened with the PBO fibers, where the load distribution among, in this case, eight bundles was non-uniform, being represented in the displacement registered in the different LVDTs placed at the bottom and top of the specimen. In this case, unlike PBO fibers, the displacement at the bottom was negligible and the displacement differentiation was not possible to be observed. However, at the top of the specimen the displacement registered at position B was slightly lower than the one registered at position A (figure 45), resulting in a slight rotation in counter clockwise direction. Based on this, is possible to stablish the non-uniform load distribution

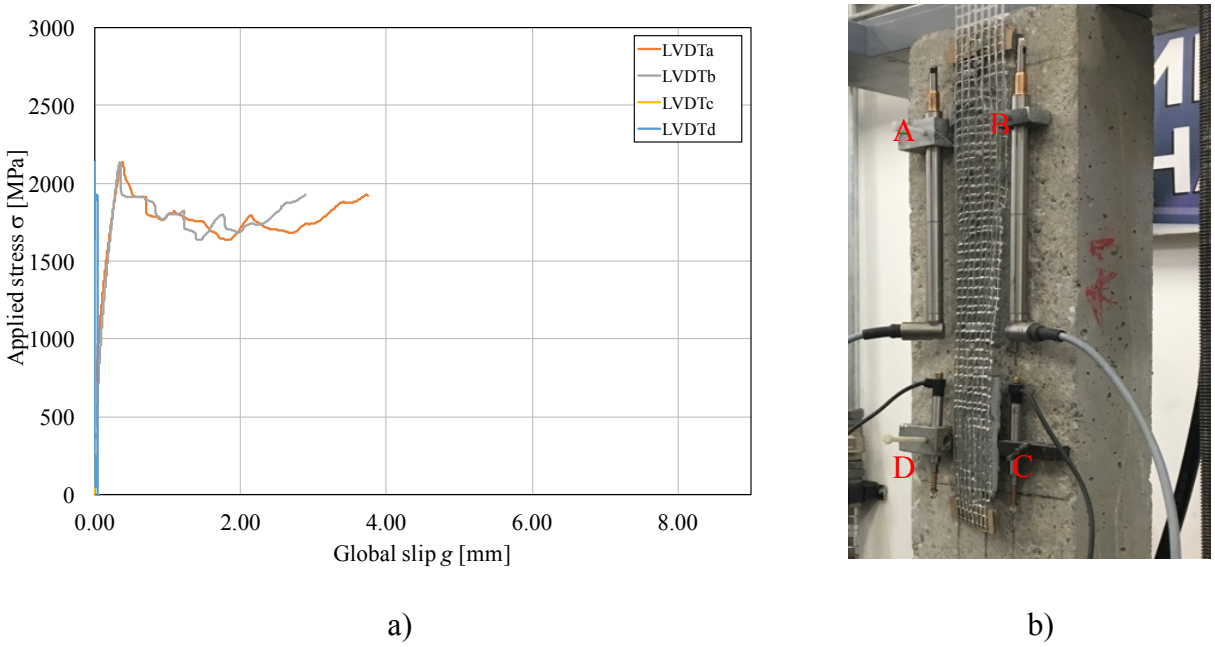

a) b)

Figure 46 a) Stress-Slip results of the four LVDTs; b) nomenclature for the LVDTs position

Due to the nature of the steel fibers and its weight, the way of casting can lead to more noticeable difference in the results in terms of ultimate strength. This influence can be noticed on the figure 47 where the dash line represents the specimens casted from top and the continuous line corresponds to the specimens casted from the bottom. For specimens four, five and six (casted from top) the ultimate strength is considerable higher than the specimens one, two and three (casted from bottom).

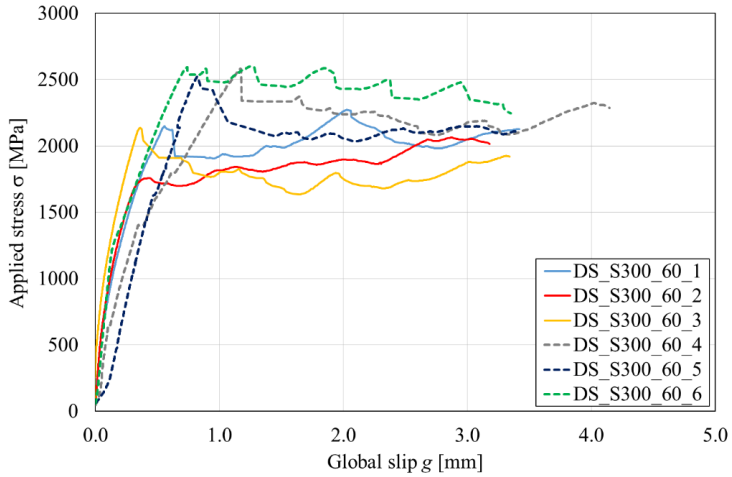

Figure 47 overall results of the six specimens

	σ_{max} [MPa]	Avg σ_{max} [MPa]	CoV
DS_S300_60_1	2275		
DS_S300_60_2	2065	2159	4.94%
DS_S300_60_3	2137		
DS_S300_60_4	2585		
DS_S300_60_5	2524	2570	1.58%
DS_S300_60_6	2601		

Table 5 Results in terms of ultimate strength

Comparing the results obtained for steel and PBO fibers, although a steel textile on average presents a higher ultimate strength than the PBO fibers, its behaviour is brittle leading to explosive failures, as it was observed during the different tests, while the PBO textile exposed a ductile behaviour.

In the table 5 is reported the ultimate strength and strain related to the concrete specimens strengthened with the FRCM using steel. The value *n* refers to the number of bundles which the textile contains. The materials and parameters used for these six tested specimens were the same except for the way how the FRCM was applied on the prisms.

Type	**Name**	**n**	**Strength [MPa]**	**ε max**
	DS_S300_60_1	8	2585	0.01305548
	DS_S300_60_2	8	2524	0.012747558
Steel	DS_S300_60_3	8	2601	0.013137135
	DS_S300_60_4	8	2275	0.011487843
	DS_S300_60_5	8	2065	0.010428648

DS_S300_60_6	8	2137	0.010793021

Table 6 Results in terms of ultimate strength and strain

Regarding to the brittle behaviour of the steel fibers, the displacement at the free end of the textile at the bottom of the FRCM is negligible (figure 48), and it is because once the debonding phenomenon takes place, the FRCM explode. Unlike PBO fibers, the steel textile does not perform a softening phase once the peak load is reached, having a sudden failure mode, leading in some cases to the impossibility to carry out its implementation.

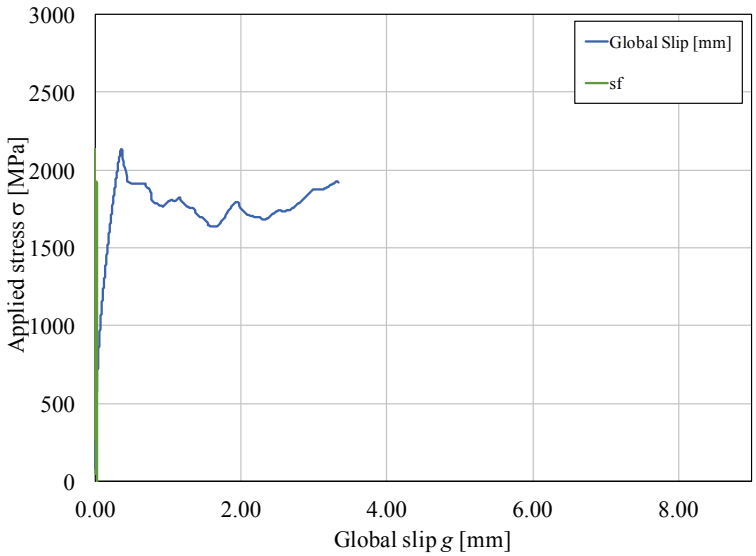

Figure 48 General steel-FRCM behavior

3. ANALYSIS OF THE LOAD DISTRIBUTION IN PBO FRCM COMPOSITES

3.1. Introduction

Traditionally, the determination of key aspects of the bonded composites such as load-carrying capacity of the interface and the interfacial shear stress-strain relation have been done by the use of contact measurements using linear variable displacement transducers (LVDTs). This instrumentation has been used to determine the global slippage and the strain in the longitudinal fiber at predetermined locations (C. Sabau, 2017). The global slippage *g* presented in this document corresponds to the average of the measurements registered by the two-top LVDTs (A and B) attached to the bare fiber net just outside of the composite loaded end.

Although the contact measurements describe the general behavior of external bonded composites certainly good, it can be challenging when considerations regarding to crack issues on the surface of the matrix, non-uniform load distribution among the different bundles and such start being considered (C. Sabau, 2017). Thus, the variability exposed in the different results using a contact measurements may be related to the named factors.

As a result of the multiple issues at certain point that a contact measurement method can encounter, a photogrammetry, which is a non-contact method, result as an innovative solution. Basically, this non-contact measuring approach identifies different coordinates of points and/or patterns using imaging sensors at different stages (figure 49). Within the photogrammetry is possible to find techniques such as point tracking (PT) and digital image correlation (DIC). The method used for the present job was DIC, and it basically works with gray-scale variations of a continuous patterns, that in this case was a high contrast stochastic sprayed, using digital images during the test execution. This results in an identification of multiple subsets, making possible the measurement and relative displacement from their initial position. To calculate this relative displacement, a computational grid is defined on a portion of the picture where the stochastic spray was made. The pictures taken before and after the deformation are correlated, making possible the measurement of the displacement of the points (figure 49).

Currently exists different correlation criteria, and depend mainly upon the computational effort required and the robustness desired. Thus, recent works have suggested and according to their results and their reliability, the use of zero-normalized sum of squares differences. The proposal to improve the correlation was not only use two pixels, but two subsets of pixels centred at each point. The shape of the subsets can be defined as s square or circle, and their sizes usually varies from 5 pixels to 50 pixels. These sizes are defined according to the robustness desired and the computational capacity. Thus, increasing the size, the computational effort increases as well as the reliability and accuracy, having a more robust analysis. Based on this, the deformation of the defined points on the grid correspond to the distance between their initial position at the un-

deformed shape and at the deformed image. Additionally, is necessary to define an extra point (Q), which provides the deformation of the subset, having at the end the total deformation of the real specimen (Marcin Tekieli, 2016).

The distance between the different defined points typically is measured in pixels, which in a further step is converted into millimeters. Nevertheless, to carry out the conversion to millimeters, it is necessary to consider either the resolution of the optical sensor or using at least one real dimension (Marcin Tekieli, 2016).

Finally, to fully implement this set-up is necessary to first, perform a speckle pattern which should be spread all over on a previously defined white background. The size of the spots/points spreaded will influence the accuracy of the result. Hence, if the spray-points process on the white background cannot be realized highly precise, artificial points placed on the fibers may be an applicable option.

Regarding to its implementation, is relatively easy, and currently the variety of image correlation systems is wide enough.

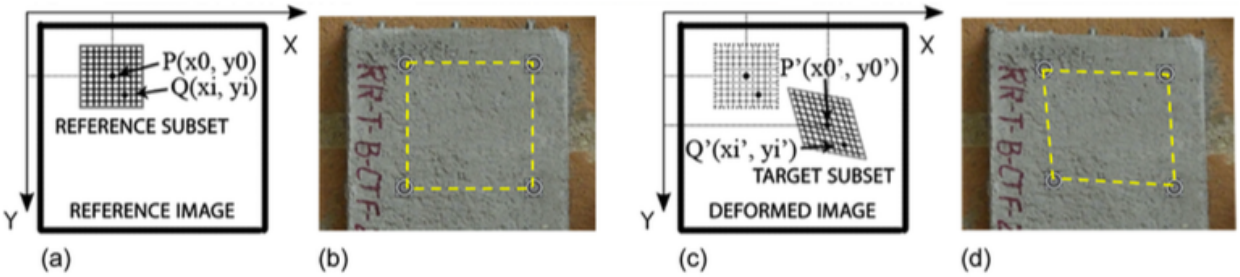

Figure 49 Principle of the image correlation system a,c) sketch of the subset; a,b) before and c,d) after deformation. Taken from *(Marcin Tekieli, 2016)*

In this section, the results obtained using DIC are presented as well as their corresponding comparison with the results obtained using the traditional LVDTs system.

3.2. Procedure

The set-up used for the image correlation analysis (figure 50) was the same that the one used for the traditional analysis using a contact measurements, but adding a camera linked to a photoshoot software, where the time step for each picture was defined. For the present job, the time step was defined every 20 seconds during the test.

The white back ground was prepared using white paint, where afterwards the different spots (figure 50) were sprayed using a black spray. During the different tests, on average, 150 pictures were taken.

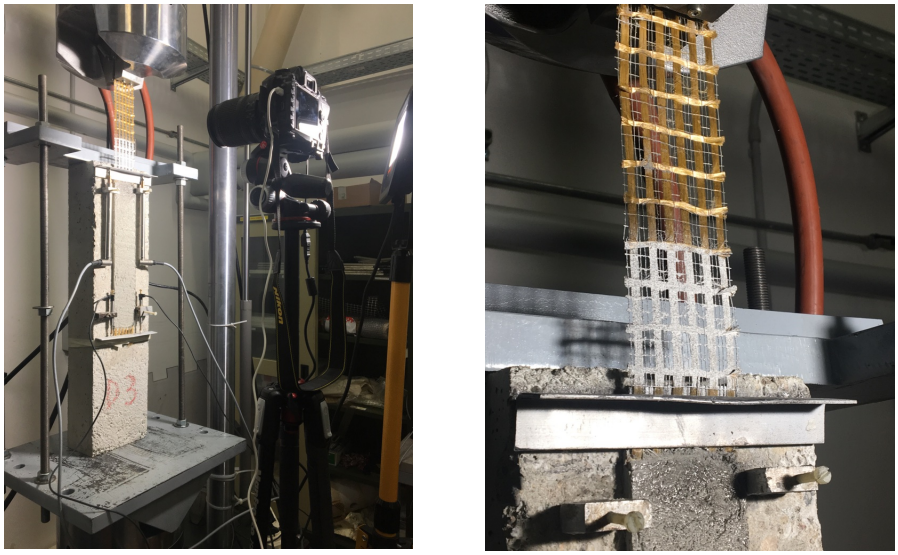

Figure 50 General set-up for the DIC analysis. White paint was sprayed on the textile

Once the experiment was finished, the post-processing process of the corresponding pictures was carried out using Vic-2D, which as an out-put, provides the displacement of the spots defined on the previous step (figure 51). Parallel, using Photoshop, were defined among the different bundles the squares, at the top and bottom, which were going to be analyzed using their coordinates (figure 51). Initially the size of the squares (subset of pixels) was 2mm x 2mm for all the bundles including the bottom and top ones. Consequently, the grid necessary to perform the analysis was fixed within the subset with 36 smaller squares, increasing with this the level of accuracy, having a more detailed grid, where the overall displacement will be composed by a considerable higher number of pixels. Furthermore, as it was explained before, the picture selected was the un-deformed picture, being the reference for the rest of the test. Hence, the next step was corroborating the corresponding relative displacement occurred during the test, using the pictures taken at every 20 seconds. To do so, the coordinates in millimeters selected using Photoshop were correlated to the coordinates resulting from the analysis carried out using Vic-2D.

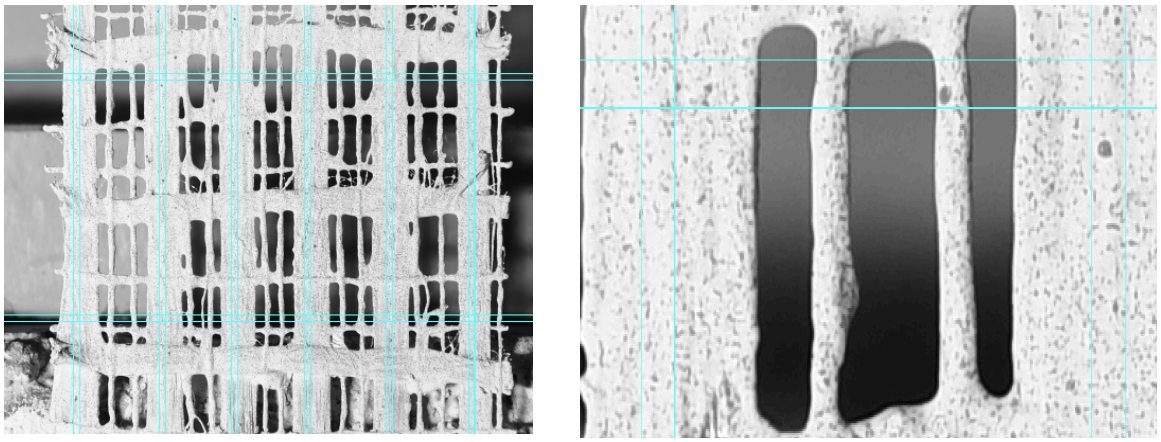

Figure 51 Definition of the subsets on the pictures taken during the test execution

Additionally, in order to fully ensure that the process implemented by Vic-2D was in concordance with the displacement observed in the different pictures taken during the test, a MatLab code was used, allowing to obtain the corresponding slip regarding to the chosen locations by means of automatic post-processing, simplifying with this the correct understanding of the mechanical behaviour of the material. This result is composed by two columns, the first representing the displacement of the top part of the bundle, and the second the bottom one. This data was initially in pixel measures, being necessary its conversion to millimetres.
This process was continuously done for the six different bundles for each one of the specimen tested.

In addition, the machine used for the test provides the data every 0.20 seconds, which differs to the time step set for the camera, which was 20 seconds. Hence, to carry out a correct comparison among the results obtained by the machine, using LVDTs and by the DIC analysis, was necessary to perform a correlation between the data, considering the force applied every 20 seconds, linking it afterwards to the displacement measured using Vic-2D, where the different pictures were analysed. Nevertheless, this procedure was not performed only for the data corresponding to the force [Kn], but also for the data recorded by the different LVDTs placed on the top and bottom of the specimen, resulting in a complete and more reliable comparison between the different data collected performing the two different procedures.

On the figure 52 is summarized the procedure followed to perform the DIC analysis with its comparison to the results obtained by the traditional method.

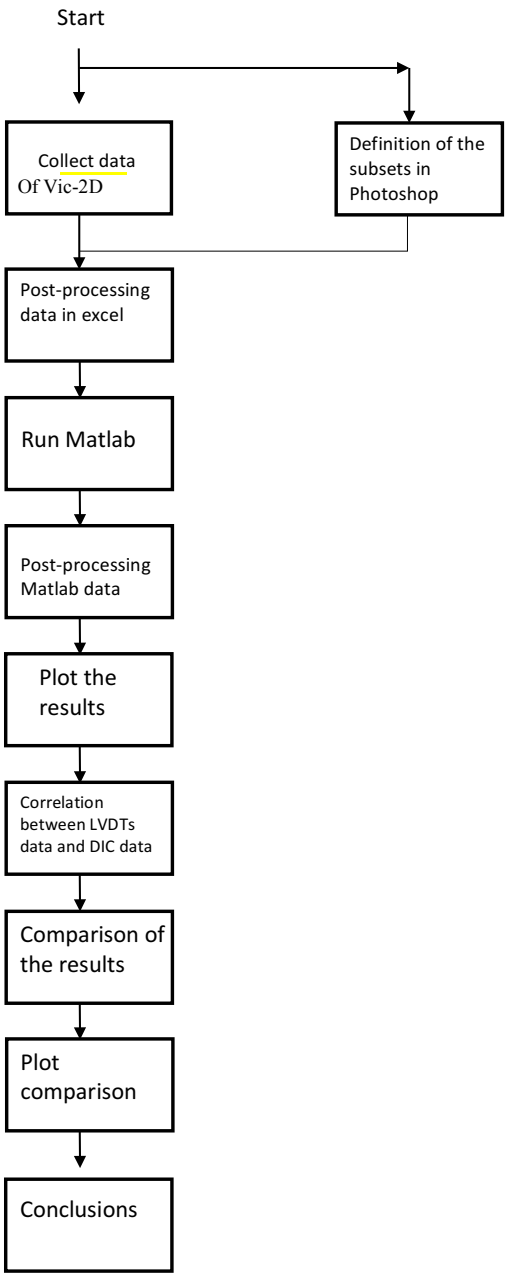

Figure 52 Procedure for DIC analysis

Despite the different measures taken performing the different tests, in some cases (shown in the following pages) the correlation of the spots sprayed on the white background painted on the textile was lost, and the results corresponding to some bundles' displacement are out of range without a

remarked tendency, being no comparable at all with the results obtained using the LVDTs, reason why some data could not be considered.

3.3. Results

For the following information and graphs presented, the nomenclature to identify the six different bundles is defined in the figure 53. Initially, apart from the assumption that the load distribution was not uniform among the bundles, the main aim and reason why the image correlation analysis was implemented, was to know in an accurate way how much stress each bundle is subjected to and decrease substantially the level of uncertainty regarding to the load distribution.

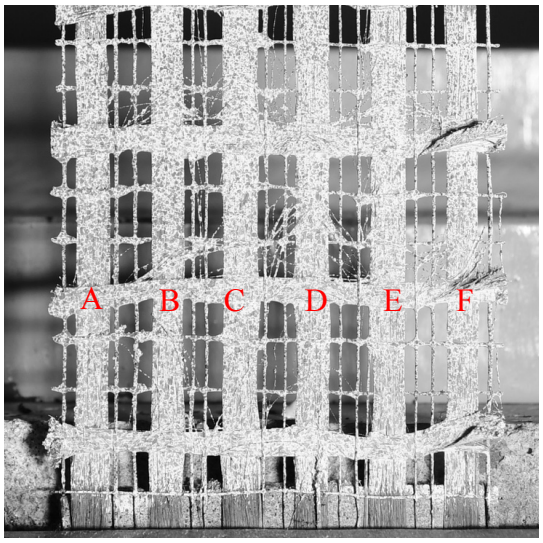

Figure 53 Nomenclature for the different bundles

Carrying-on, the results obtained after the DIC analysis are presented in the following section, being identified with the nomenclature DS_300_60_X, where 300 represents the length of the composite in millimetres and 60 the width. Additionally, X correspond to the number of the specimen tested, from 1-6.

In the graphs presented where the data collected from the DIC analysis and the LVDTs is compared, the stress (sigma σ)was calculated multiplying the strain based on the DIC data by the nominal Elastic modulus (E) of the textile.

- DS_300_60_1

As an initial result, the distribution of the load among the six bundles was the one shown on the figure 54, where the result obtained using the LVDTs was corroborated. Additionally, is possible to check the stress that each bundle is subjected to and its corresponding displacement.

For certain bundles, especially the F, the correlation was lost at certain point, making impossible to see indeed how the load was distributed along the yarn.

Once this behaviour was observed, the process was performed again, with the purpose of obtain an improvement in the final result. Initially one of the assumptions was that this correlation-loss could have been due to the lack of sprayed-spots on the chosen zone. Hence, the subsets along the F yarns were re-located, changing its coordinates, being necessary to perform the entire process again. The results were the same, and near to the possible peak load that the yarn could approximately achieve, based on the results obtained on the other bundles, the correlation was lost.

Despite the correlation loss for some bundles, one of the aims was to compare the results in terms of stress-displacement obtained using the LVDTs and the results obtained using DIC system. It is evident in the figure 54 how the tendency is kept in some zones of the textile.

Since Vic-2D primary needs the different spots to evaluate their corresponding displacement during the test, the phenomenon observed along the yarn F may be due to the lack of accuracy at the moment when the spray was applied on the white back ground. Nevertheless, the result obtained shows clearly how different may be the load distribution among the yarns, contributing to the enhancement of the understanding of the FRCM materials´ behaviour.

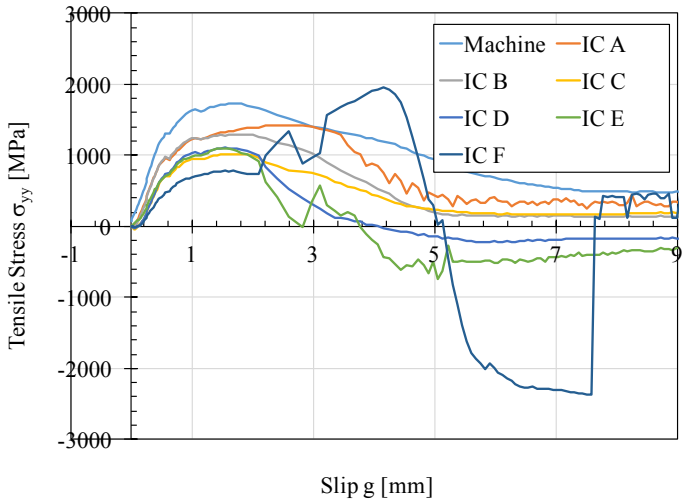

Figure 54 Strees-slip relation among the bundles

In addition, with the data obtained through the implemented analysis, the differentiation of the displacement in relation with the different locations (top and bottom, figure 55) along the different bundles was possible to carry on.

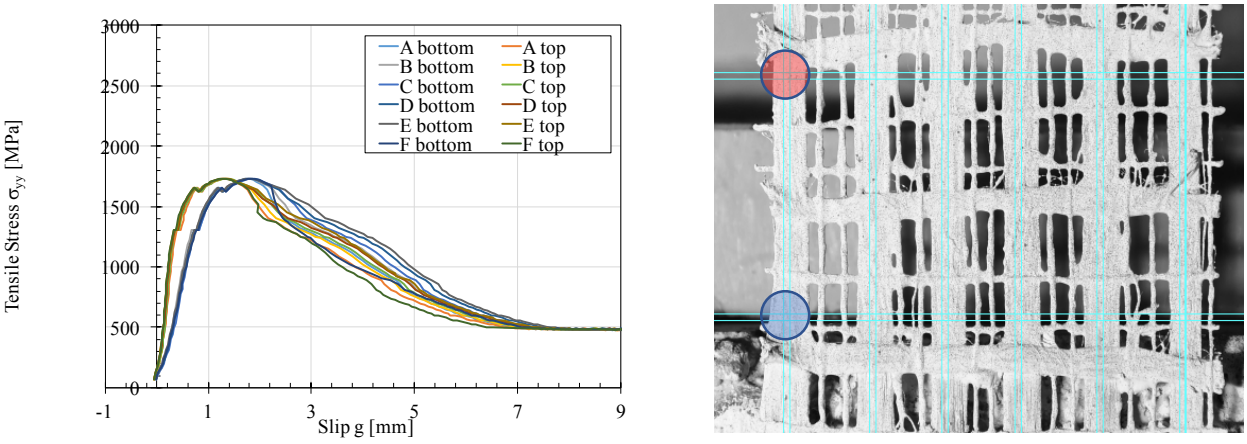

Figure 55 Top and bottom slip

On the figure 55 is highlighted the different locations considered during the execution of the analysis, where the red circle represents what in the figure 55 is called top, and the blue circle represents what in the figure 55 is called bottom. Noticing more in detail the figure 55, there is a clear marked tendency among the top a bottom displacements, resulting the bottom slightly higher, and it is due to its location, which is closer to the loading end. In order to make this minor but considerable difference noticed, the range of colours of the series representing the bottom behaviour is dark, while the one representing the top behaviour is lighter.

The result obtained was considerable close to the one expected before the test and post-processing execution, being significant close to the one reported in the literature.
On the other hand, and in order to make easier pointing out the non-uniform load distribution among the different bundles, a bar diagram is presented (figure 57) where the different bundles are discretized along the X axis, being possible the observation of the result desired at the beginning.

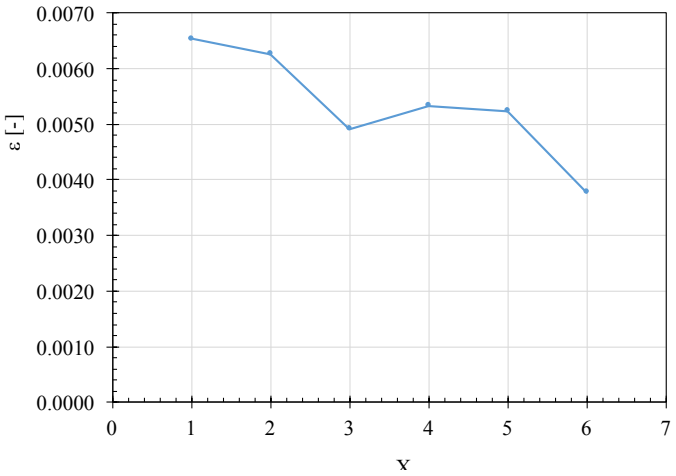

Figure 56 load-distribution in terms of strain

In the figure 56, the load distribution is presented in terms of strain, in which is clear the difference in deformation presented between the yarns that is represented from 1-6 (where bundle 1 corresponds to the data of bundle A, and bundle 6 corresponds to bundle F)
The results, in terms of load distribution, corresponds to the distribution observed when the specimens reach the peak load (debonding occurs).

Is highly important to notice that since the correlation during the DIC analysis of the bundle F (6) was lost, its result is plotted but it is not considering within the conclusions or assumptions derived from the analysis. For this case, in which the load distribution is presented in terms of strain, the bundle number 3 (C) presents the lowest value among them. Implying with it, that this bundle is the one subjected or supporting less stress than the others. According to the figure 57, is possible to concur that the third bundle evidently, in terms of stress, is the bundle supporting less load than the others.

Concluding with this that the bundle subjecting to a higher load among the others is the bundle 1, followed by the bundles 2, 4, 5 and 3.

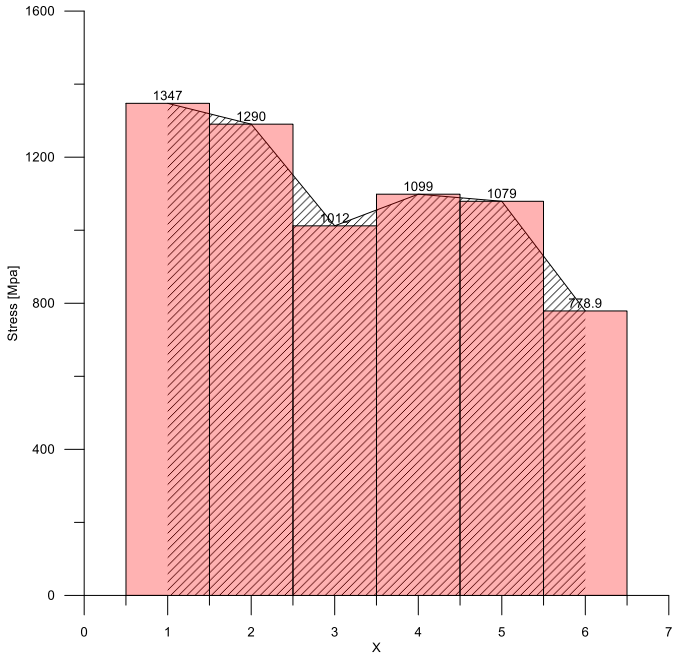

Figure 57 load distribution in terms of stress

Additionally, is possible to present the non-uniform load distribution exposing the slip experienced by each bundle at certain point, in which in this case is the point where the peak load is reached. As well as the different stress distribution among the bundles was noticed, in the figure 58 and 59 the displacement regarding to the points initially selected (top and bottom) is presented.

Looking at the figure 59, the displacement experimented by the bottom location is slightly higher than the one registered at the top part of the textile, due mainly to its location. The bottom point initially selected was closer to the loaded end, being in this way subjected to a higher displacement during the test execution. Moreover, the results in terms of displacement concur with the stress distribution along the textile, being the bundles that support the major part of the load, the ones which experiment less displacement.

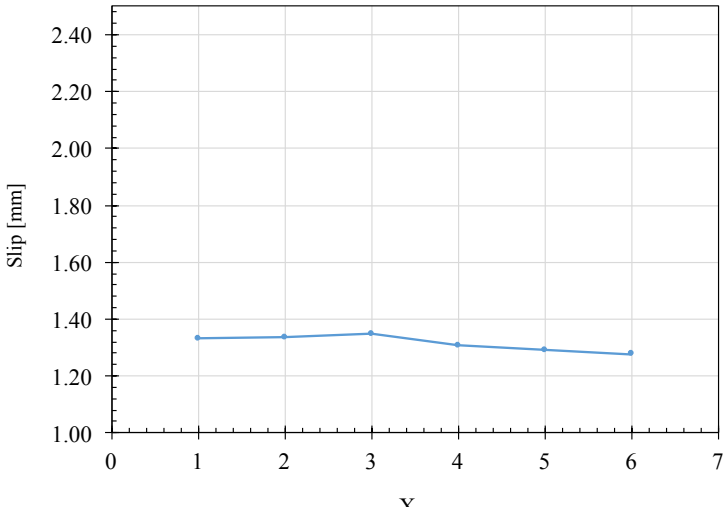

Figure 58 Slip of the top part of the textile

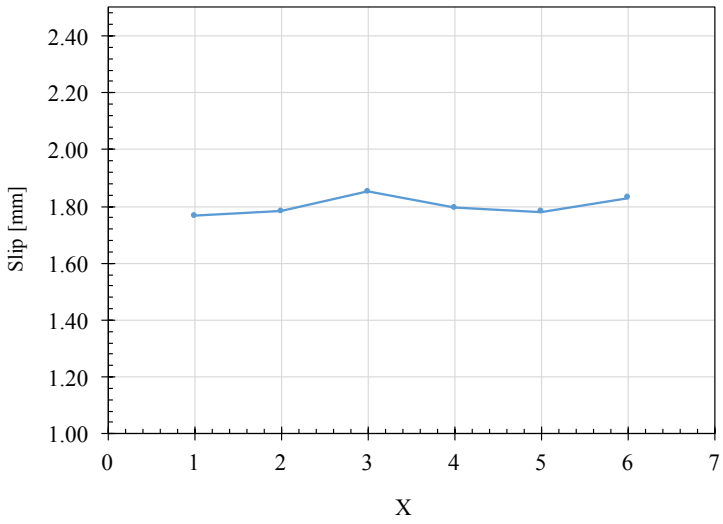

Figure 59 Slip of the bottom part of the textile

- DS_300_60_2

For some specimens, the correlation in all the bundles was lost (figure 60), and the reason may be attributed to the lack of precision at the moment when the spray was applied on the white back ground. Additionally, the light conditions should be kept stable during the test execution, and to assure this, the use of LED light is strongly suggested, offering highly better conditions than the incandescent lamps. However, the resolution of the camera can affect in a great manner the final results as well as its support, which should be stiff enough to guarantee the parallelism during the execution time (Marcin Tekieli, 2016).

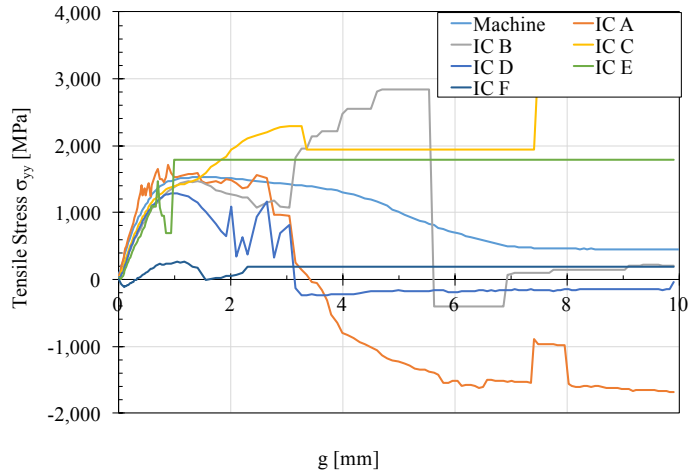

Figure 60 stress-slip relation among the bundles

Due to the non-encountered correlation during this specimen execution, the bar diagrams presented for the first specimen was not carried out, implying the non-consideration of the data regarded to this specimen.

- DS_300_60_3

Following the same process exposed for the first specimen, a corresponding comparison between the data collected from the LVDTs lectures and the one from Vic-2D was made, evidencing again the non-uniform load distribution among the yarns which compose the textile. In the figure 61 is evident, as it happened in the specimen 2, that for some bundles the correlation was lost, completely or partially. For instance, the correlation for the yarn B was kept until certain point and after the peak load was reached the further data lost totally the tendency that it should have followed. This phenomenon was present for bundle E and C as well. The data regarding to the yarn C was decided not to plot due to its out-of-range values, losing the proportion of the remain data corresponding to the other bundles, making extremely difficult pointing out the different results.

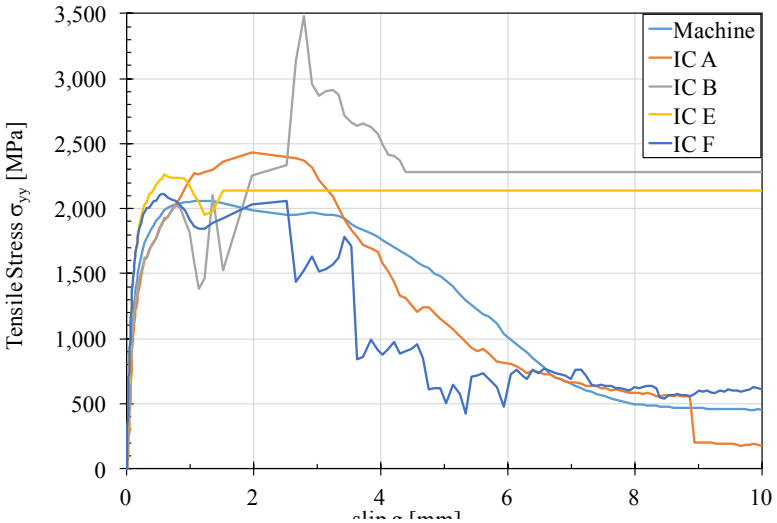

Figure 61 Stress-slip relation among the bundles

In accordance to the initial intended objectives, as it was carried out for the first specimen, the differentiation between the locations (top and bottom) among the different bundles was made, as it can be observed in the figure 62. Once again, the different range of colours was implemented, being suitable to the correct and easier identification of the different data presented.

On the figure 61 is highlighted the top and bottom subsets in red and blue circles respectively. As it was expected, the location closer towards the loaded end present a higher displacement comparing to the one located at the top part.

In this case, the difference in terms of displacement between the top and bottom locations in the six different bundles was more noticeable, and is due to the peak stress reached, which for this case was near to 2000 Mpa, unlike the one reached during the first test that was around 1700 Mpa.

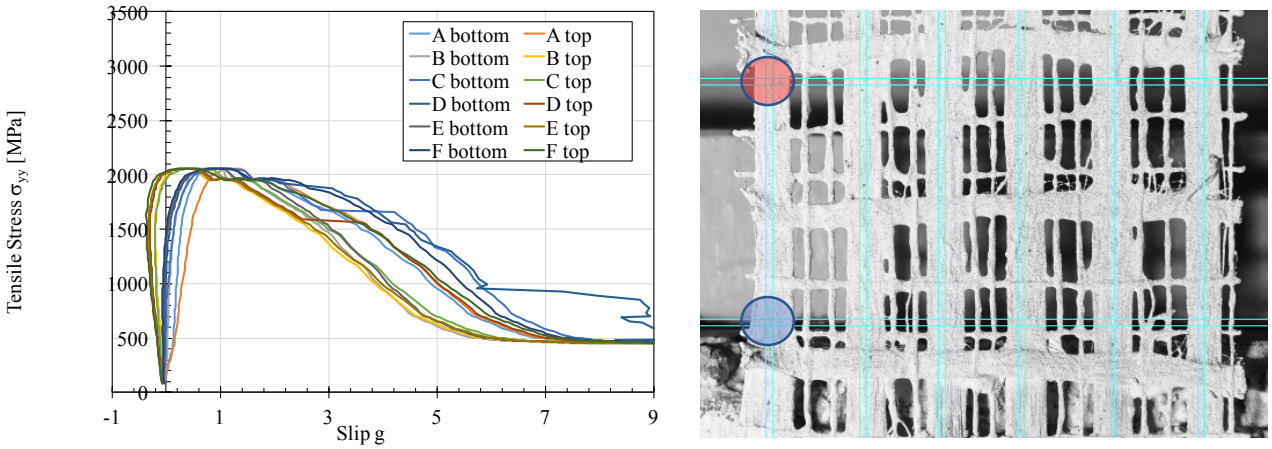

Figure 62 Top and bottom slip

Thus, despite the same nominal mechanical features of the materials involved in the test execution, the results in terms of peak load and deformation can present in some cases substantial differences.

Additionally, the distribution of the load in this case, as it was expected, was a non-uniform distribution, being some bundles subjected to a higher stress than others (figure 63). It is important to notice, that for instance in the specimen one (DS_300_60_1), the bundle which support the major part of the load is the first, unlike the third specimen (DS_300_60_3) where the bundle four is the one supporting the major part of the load.

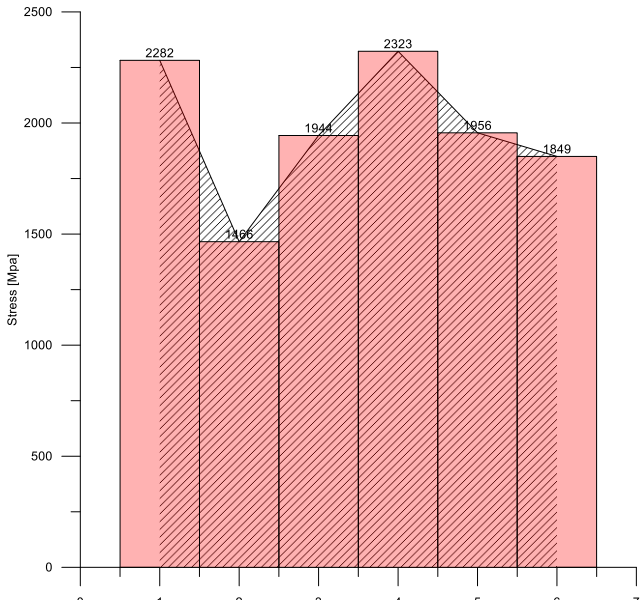

Figure 63 Load distribution in terms of Stress

As well as it was performed for the previous specimens, the non-uniform load distribution considering the differentiation in terms of displacement suffered by the different bundles (figure 64 and 65), can lead to similar conclusions, evidencing the bundle which support most and less part of the load applied.

Comparing both results obtained after perform IC analysis, the bundle which support the most part of the load in terms of stress, has a minor value of displacement compared to the others.

The results obtained show the same behaviour experienced with the other specimens tested, where the location closer to the loaded end, is more susceptible to experiment a higher displacement.

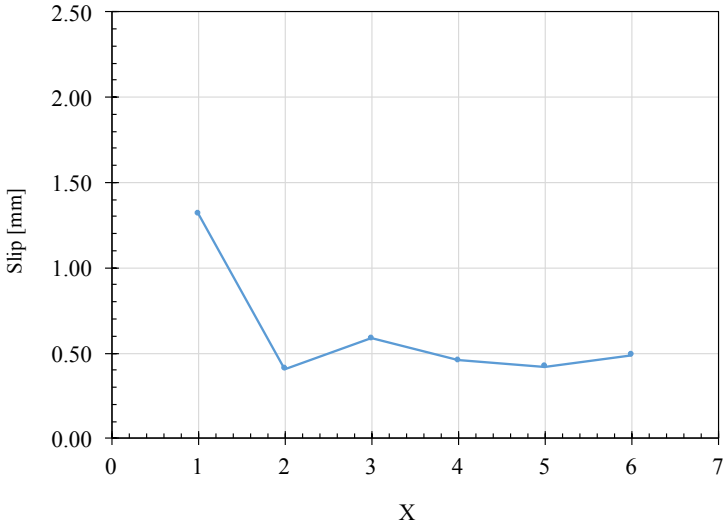

Figure 64 Slip of the top part of the textile

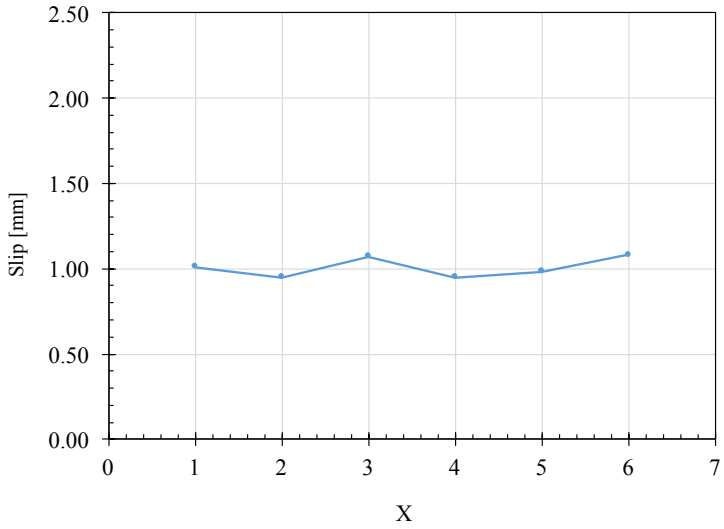

Figure 65 Slip of the bottom part of the textile

- DS_300_60_4

At this stage, the process may be result repetitive, but considering the major variety of inconveniences that it can encounter, was essential to perform the procedure described for the different specimens, especially when it was observed that for some of them the results were not totally satisfactory.

As it happened with the results of the second specimen (DS_300_2) and at certain point of the third specimen too, in this case the correlation for some bundles near the peak load was lost.

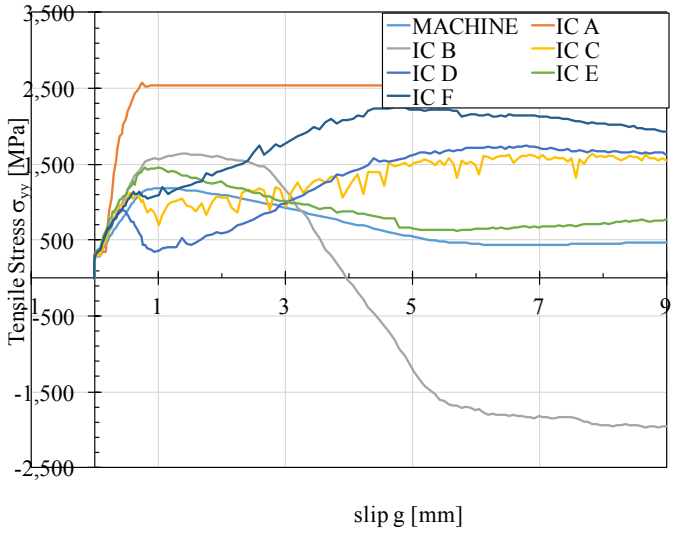

Figure 66 Stress-slip relation among the bundles

The phenomenon observed on the figure 66 was repetitive in other specimens. In this case specifically, the data corresponding to the major part of the textile (all the bundles excepting E) follows certain tendency until the peak load is reached. Nevertheless, the differentiation in terms of displacement was according to the assumptions made before the test execution (figure 67).

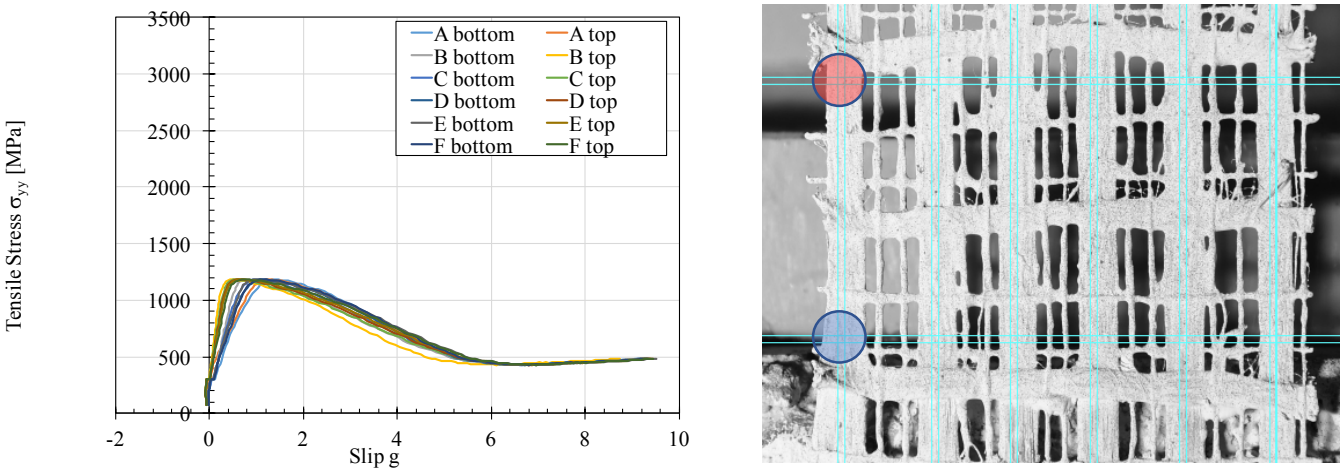

Figure 67 Top and bottom slip

Similarly, it is noticed in the figure 67 the difference among the bottom and top displacement, being the bottom location the closest to the loaded end, experimenting firstly the effect of the applied load.

As it happened in the previous tests, the distribution of the load among the different yarns of the textile was different showing a clear re-distribution (figure 68). As is it noticed, for this specimen major part of the distribution occurred along the first bundle, unlike specimen three (DS_300_60_3) where the major part of the load was supported by the second (B).

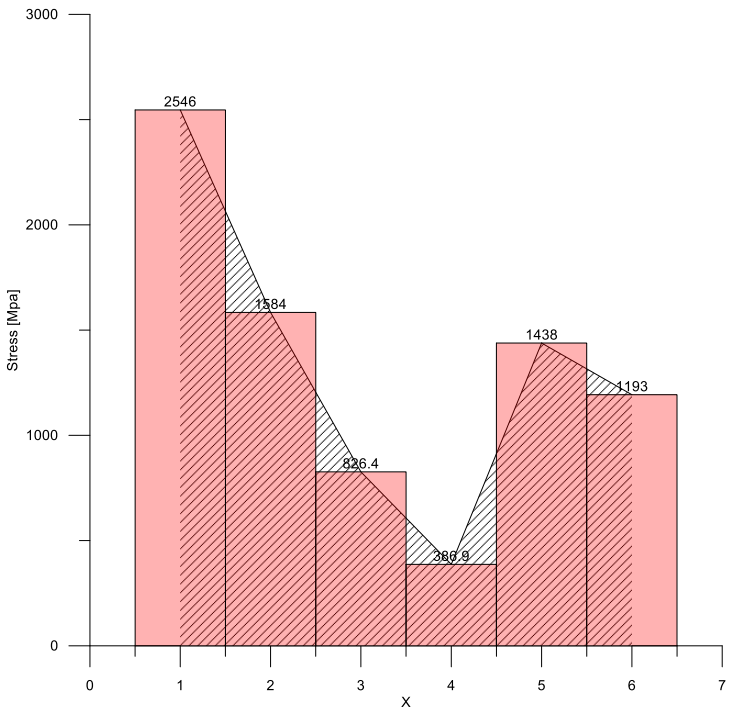

Figure 68 Load distribution in terms of Stress among the bundles

Similarly, the analysis in terms of displacement was carried out, and the results confirmed the results obtained in terms of stress. The behavior presented in the figure 69 and 70 shows the theoretical relation between the displacement and stress, in which the bundle supporting the major part of the applied load, experiments less displacement.

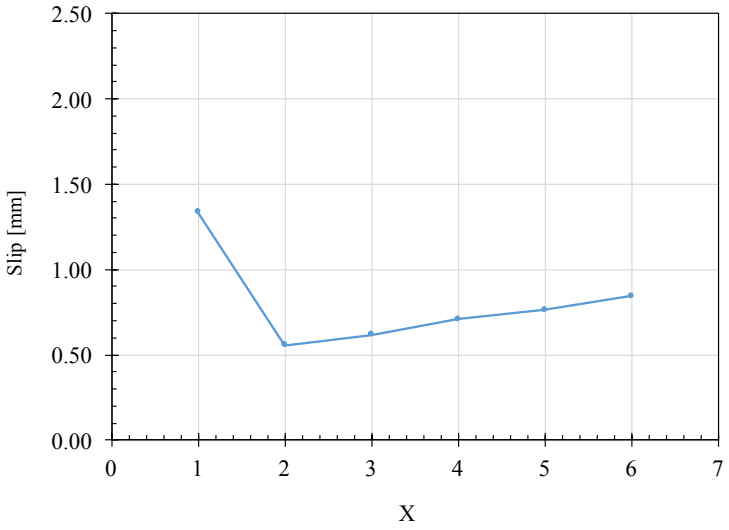

Figure 69 Slip of the top part of the textile

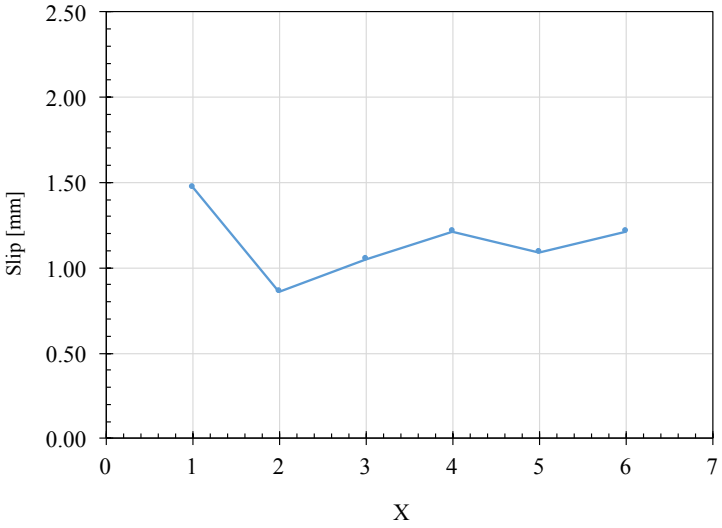

Figure 70. Slip of the top part of the textile

- DS_300_60_5

In concordance to the procedure exposed, the analysis of the fifth specimen was carried out, where the similarities noticed during the others tests where present in this one too. Indeed, the mechanical behaviour and load distribution was evident, but as it happened in the major part of the specimens, the correlation at certain point was lost, in this case this phenomenon was more evident along the last bundle (F), where after a certain point, the stress supported by the bundle remain constant until the end (figure 71).

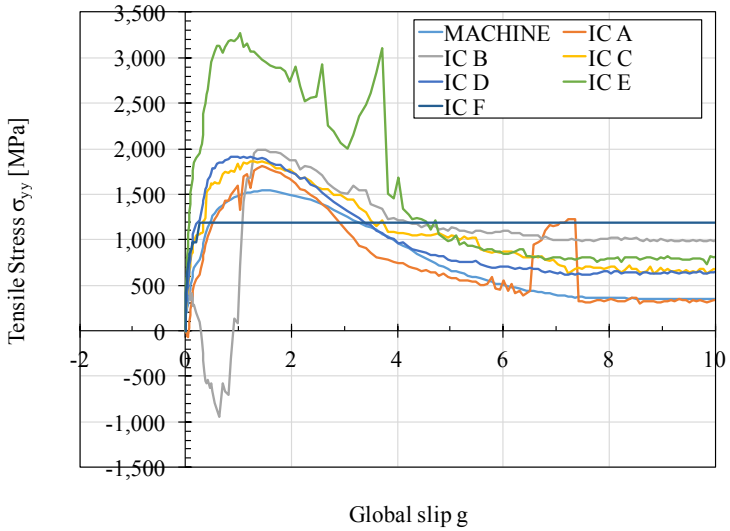

Figure 71 Stress-slip relation among the bundles

Although the correlation along the F bundle was lost after certain time, the tendency followed by the other curves was similar among them. The behaviour observed along the E bundle clearly is out of range according to the previous results obtained, but its trend follows the same that the one reported by the LVDTs measures. Similarly happened to the bundle B, where initially its strength values were negative, and immediately after its trend was the one expected.

The peak load achieved did not vary significantly among the different specimens, depending mainly upon the bond behaviour at every interface, which depend at the same time on the different precautions taking during the casting process.

As it was performed for the other specimens, the comparison between the top a bottom displacement was carried out, in which the tendency observed during the test 1-4 was noticed in this as well (figure 72).

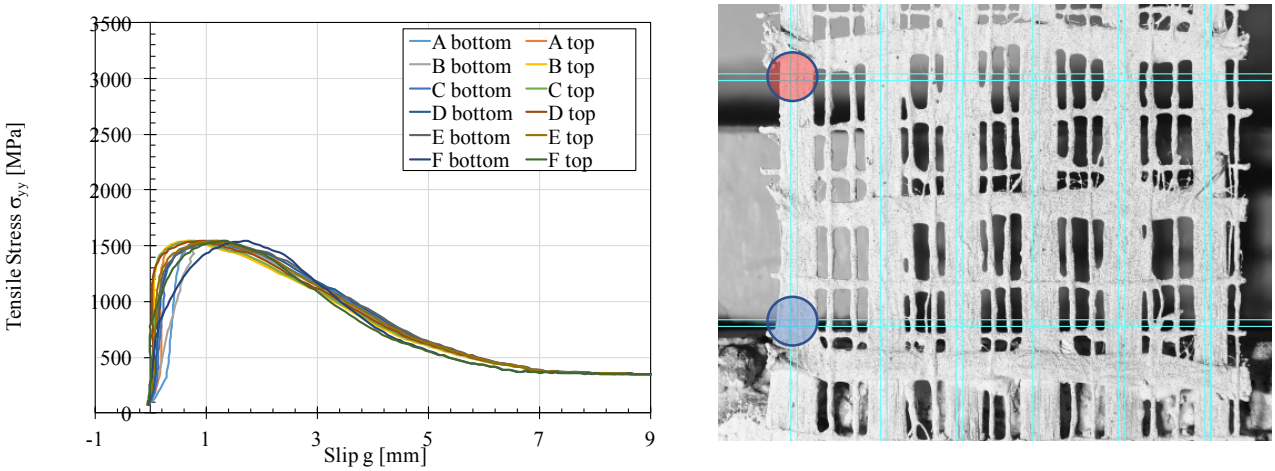

Figure 72 Top and bottom slip

Its trend regarding to the top and bottom zones behaviour was the same encountered during the execution of the other tests, being the bottom zone (closer to the loading end) the one experimenting a higher displacement.

According to the data reported and the information on the graphs, the variation in terms of maximum strength is within the range 1200-2000 Mpa, which result in a variation of about 30%.

In terms of load distribution among the different bundles (figure 71), the curves followed the general trend heading by the LVDTs data, experimenting slightly differences at certain points, generally close to the peak load. Regarding to load supported by bundle E, which is out of range, its shape unlike some other results, kept the expected tendency. However, considering a possible loss of correlation in this zone of the textile, this conclusion cannot be considered as a reliable

result. Getting rid of the data corresponding to this bundle. The yarn subjected to the maximum strength was the yarn B (2), similar to the result obtained in the previous tests where the bundle experimenting the maximum load was either the first or second.

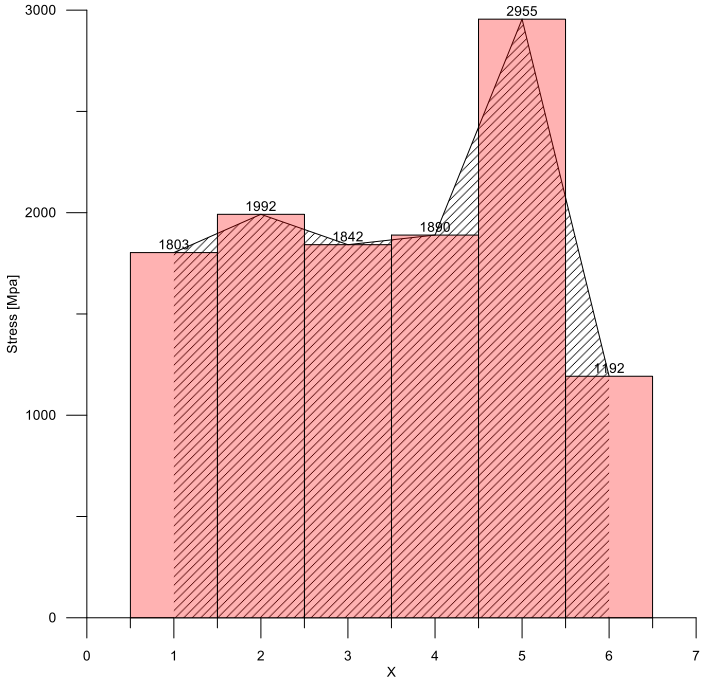

Figure 73 Load distribution in terms of Stress among the bundles

Clearly the out-of-range of the data of the bundle E cannot be considered, but it is, indeed, an indicator of the non-uniform load distribution along the different yarns which compose the textile.

Performing a displacement analysis, as it was performed in terms of stress among the bundles, the non-uniform load distribution can be noticed as well. A key behaviour which can lead to a reliable conclusion once the photogrammetry analysis would be finished, is the verification of the behaviour that in theory the material should follow. For instance, having the displacement and stress distribution of the textile, these two factors can be compared, leading to such corroboration. It is important to verify that the bundles supporting the major part of the load suffer the less slip compared to the others, which in the major part of the cases, except for bundles where the correlation was lost, did happen.

The trend observed between the displacements at the top and at the bottom is present in this test, where the bottom location in the textile, which Is closer to the loaded end, experiments a

higher displacement than the top part. The difference is not substantial, but since the fibers are not made by a rigid material, in which the load is transfer approximately uniform, the difference always should exist.

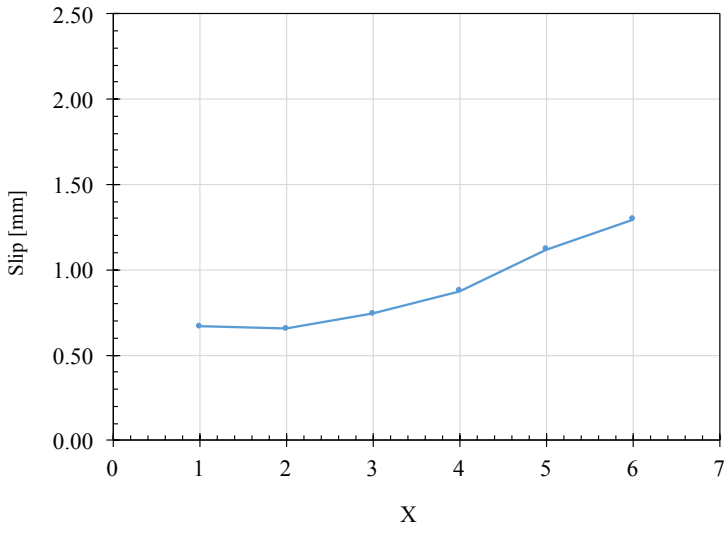

Figure 74 Slip of the top part of the textile

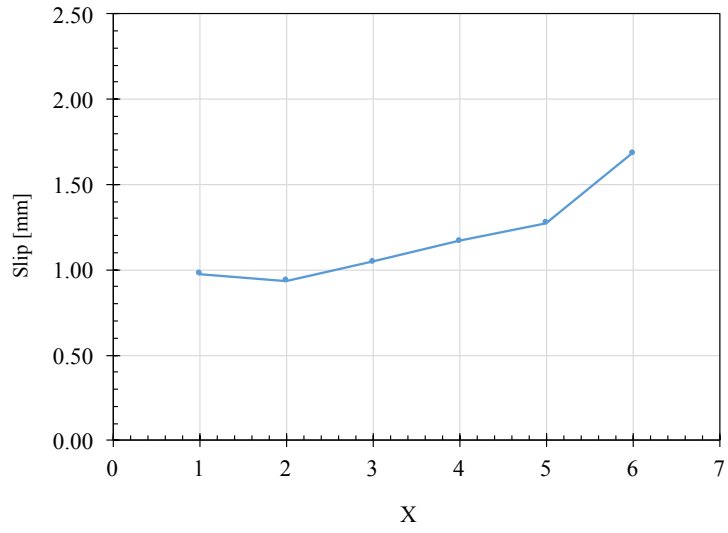

Figure 75 Slip of the bottom part of the textile

- DS_300_60_6

Regarding to the results corresponding to the specimen number six (DS_300_60_6), the pictures obtained from the camera and analysed by Vic-2D correspond only to the half of the test, being impossible to carry out a complete post-processing analysis. Reason why was decided not to plot these results, and consider only the data obtained from the LVDTs placed on the specimen,

evidencing a rotation and displacement differentiation among the free and loaded end, intuiting with it the initial assumption of non-uniform load distribution and then corroborated with the DIC analysis performed in the other specimens.

Throughout the analysis of the results obtained of the specimens DS_300_60_1, DS_300_60_3, DS_300_60_4 and DS_300_60_5, is possible to identify clearly a common behaviour. Through the photogrammetry analysis performed to the four specimens, the non-uniform load distribution was a common factor presented in the results. As it presented in the figure 76, the load distribution among the textile is different in all the specimens, but among the specimens the distribution is different as well, being difficult to stablish a certain pattern or tendency able to clarify the zones where the major part of the load would be re-distributed.

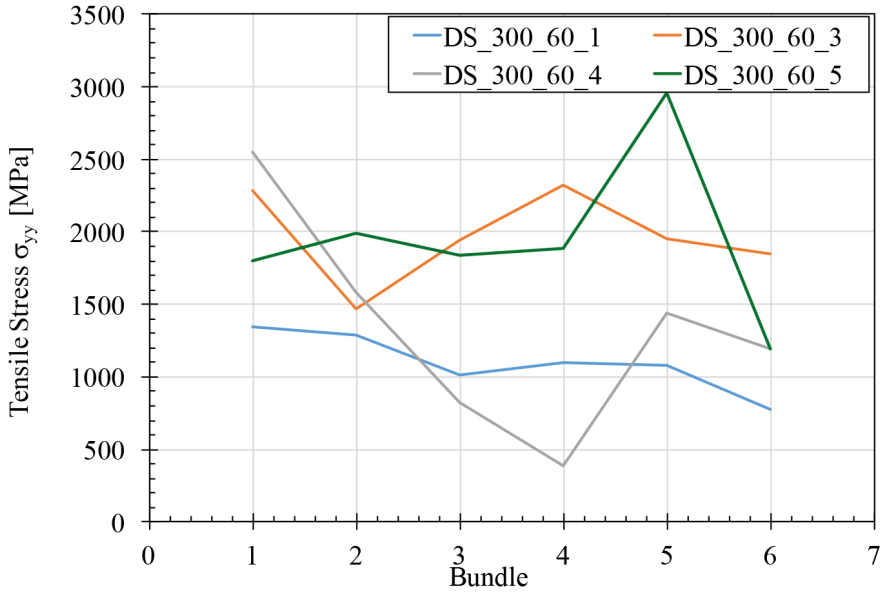

Figure 76 Final comparison among the different specimens (bundle by bundle) in terms of stress

Observing the figure 76, the distribution of the stresses among the bundles in the different specimens are diversified through the different zones of the graph with a no clear delimitation between them. Therefore, a factor which may lead to this behaviour is the impregnation grade of the mortar along the textile, having a different bonding behaviour at matrix/textile interface, resulting in a random variation in terms of load distribution, being impossible a delimitation of certain ranges among the bundles before the test execution.

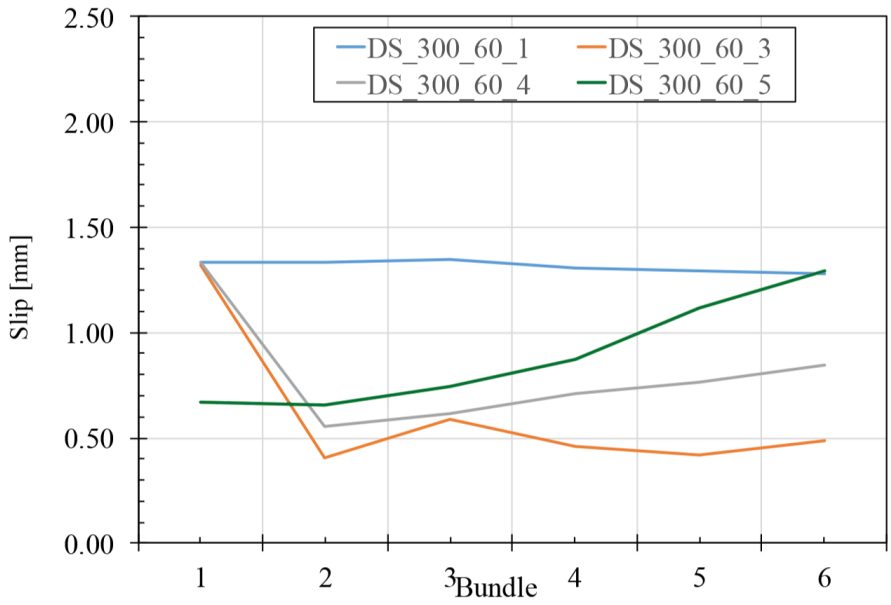

Figure 77 Final comparison among the different specimens (bundle by bundle) in terms of stress at the top of the extile

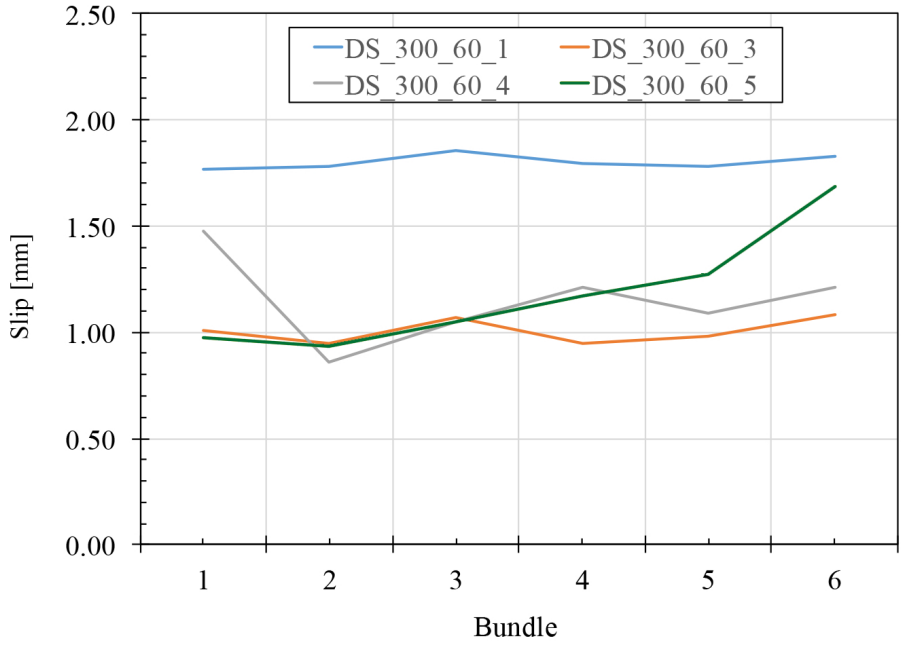

Figure 78 Final comparison among the different specimens (bundle by bundle) in terms of stress at the top of the extile

4. DISCUSSION OF THE RESULTS

Initially were defined certain parameters which according to them the final results were going to be evaluated and compared to the intended result. The very initial aim, which did motivate the implementation of the tests and such, was to evaluate how the way of casting can influence the final performance of the specimens. On the figure 31 is evident that, in the case of PBO fibers the way of casting does not influence the overall performance of the specimen, representing the dash line the specimens casted from the top and the continuous the ones casted from the bottom. The results are clearly not-well defined in specific range suggesting that the way how the casting process was carried out does not influence the ultimate strength. Despite the specimen that reached the maximum ultimate strength was casted from the top, this behavior is not repeated in the other specimens.

Unlike PBO fibers, the behavior of steel-FRCM shows a clear difference among the range where the dash line, representing the specimens casted from the top, reached a higher ultimate strength value compared to the other specimens, which in this case are represented using continuous lines. The impact on the final performance considering the casting, can be up to 20%, being the maximum load achieved by specimens DS_S300_60_4, DS_S300_60_5 and DS_S300_60_6 close to 2500 Mpa, while the one achieves by the specimens DS_S300_60_1, DS_S300_60_2 and DS_S300_60_3 was around 2000 Mpa.

Additionally, and in order to compare the results obtained using the permanent contact measurement method (LVDTs), and the digital image correlation analysis DIC, in the table 6 the values corresponding to the maximum displacement registered at the peak load are reported.

During the DIC analysis (figure 55), two different points, at the top and at the bottom of the textile, were chosen making possible to carry out the comparison and differentiation of the stress distribution along the bundle. Reason why, unlike LVDTs, on DIC analysis were considered two values. The variation between the values obtained from DIC analysis and from the LVDTs lectures for the four specimens showed are around 6%, 6%, 25% and 6% respectively, being the specimen DS_300_60_4 the one showing the highest variation among the others.

In general terms, the results, in terms of displacement, were within a range in which the results are comparable, considering also the advantages regarding to the implementation of such analysis.

Maximun displacement [mm]				
Specimen	**LVDTs**	**DIC**		
		Top	**Bottom**	**Average**
DS_300_60_1	1.7	1.348098877	1.852497939	1.600298408
DS_300_60_3	1.28	1.317316998	1.0801414	1.198729199
DS_300_60_4	1.08	1.33383436	1.474397153	1.404115756
DS_300_60_5	1.41	1.295603103	1.683153016	1.48937806

Table 7 Comparison between DIC and LVDTs results

Although the stress and displacement among the different bundles for each specimen was different, having an overall view of the results obtained, the maximum displacement that the specimens were subjected to, was obtained in specimen one (DS_300_60_1) at the bundle three. The result was repeated on both locations, top and bottom. On Table 7 and 8 is highlighted the overall maximum displacement at top and bottom.

Displacement top							
1		3		4		5	
bundle	displacement peak top	bundle	displacement peak top	bundle	displacement peak top	bundle	displacement peak top
1	1.332122103	1	1.317316998	1	1.33383436	1	0.669308957
2	1.335376631	2	0.405403702	2	0.557184972	2	0.654578283
3	1.348098877	3	0.587451816	3	0.618502112	3	0.743954393
4	1.307692008	4	0.457870244	4	0.707550012	4	0.874816891
5	1.290109102	5	0.418691732	5	0.763193572	5	1.119887206
6	1.276668323	6	0.487448039	6	0.845020552	6	1.295603103

Table 8 Displacements registered at the top of the textile

Displacement bottom							
1		3		4		5	
bundle	displacement peak bottom	bundle	displacement peak bottom	bundle	displacement peak bottom	bundle	displacement peak bottom
1	1.767415273	1	1.010211027	1	1.474397153	1	0.976621791
2	1.782419916	2	0.948076565	2	0.860315553	2	0.937089472
3	1.852497939	3	1.071315963	3	1.049697833	3	1.046126522
4	1.794212298	4	0.949628491	4	1.213018053	4	1.170766062
5	1.780644719	5	0.982140062	5	1.090960233	5	1.275804786
6	1.829082243	6	1.0801414	6	1.214261993	6	1.683153016

Table 9 Displacements registered at the bottom of the textile

Observing the table 7 and 8, is clear the non-uniformity in terms of displacement observed among the specimens and among the bundles of the specimens. regarding to the top part of the textile, unlike specimen DS_300_60_1, the firs bundle on specimen DS_300_60_3, DS_300_60_4 and the sixth bundle on specimen DS_300_60_5 were the ones supporting the major part of the load. Therefore, cannot be identified a repeated pattern between the specimens, due mainly to the impregnation grade of the matrix within the textile.

On the other hand, in the bottom part, the distribution in terms of displacement was still different, being the sixth bundle in the third specimen the bundle experimenting the maximum displacement, while in the fourth and fifth specimen the bundle experimenting the highest displacement was the first and sixth respectively. Hence, having no pattern in the distribution of the load among the

bundles in all the specimens, parameters such a permeation grade of the matrix within the textile may be considered to ensure a more uniform behaviour of the textile in the different zones.

Besides, on the figure 79 the results in terms of displacement at the top and at the bottom are showed, being possible to notice a similar behaviour between the top and the bottom curves. As it was expected, the location closest to the load application point is where the displacement is slightly higher, being in this case the bottom part of the textile. Although the displacement in the top and bottom part are different, the shape of the lines describing their behaviour may be considered consistent, evidencing the same tendency.

Despite the clear re-distribution of the load among the different bundles, for some specimens this distribution took place more uniformly than in the others. This is the case of the specimen DS_300_60_1, where the difference between the bundle subjected to the major part of the load (having less displacement) in comparison to the one subjected to the minor part (having a higher displacement), is considerable less than the difference observed in the other specimens. This difference should be within a certain range pre-determined making possible evaluate the reliability of the results obtained. This is discussed in the further pages and its possible impact on the final performance in terms of ultimate strength of each specimen.

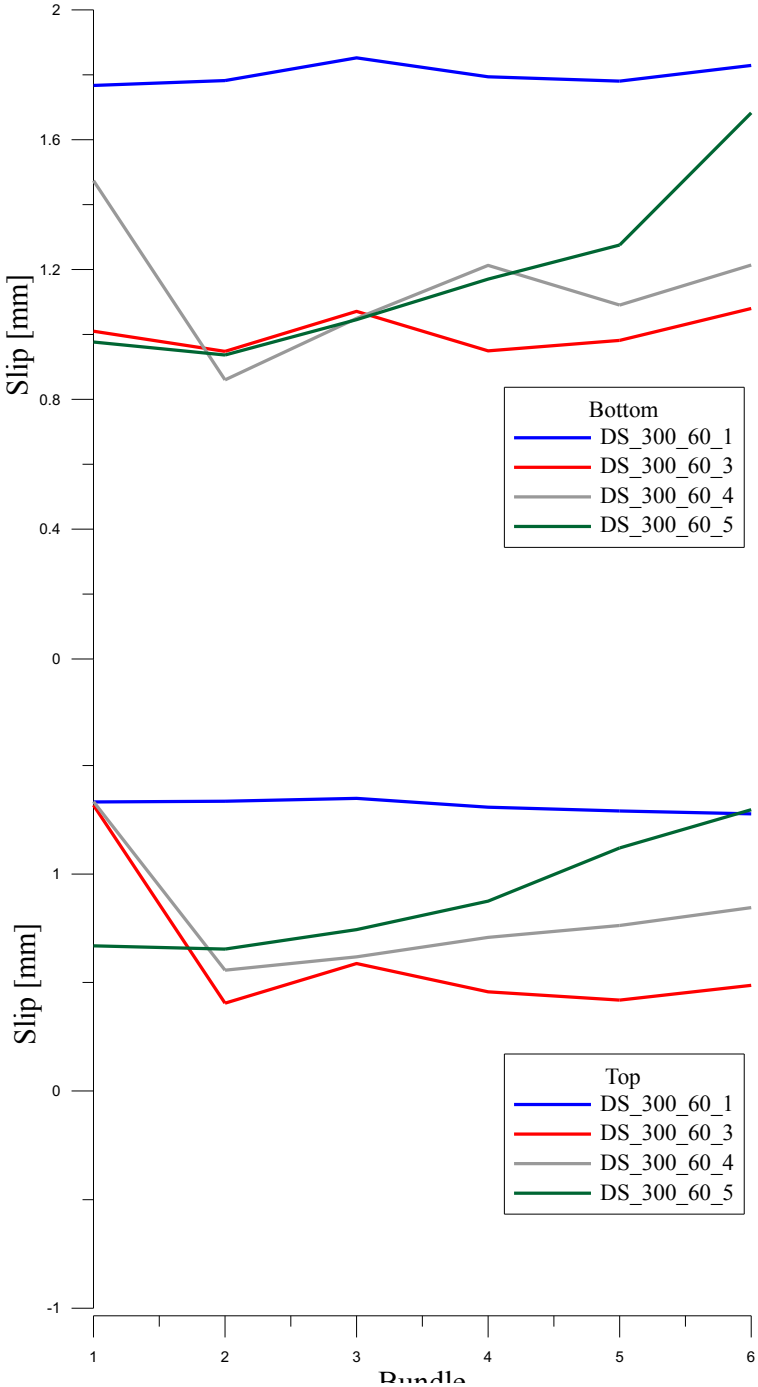

Figure 79 Final comparison between the displacements registered at the top and bottom of the different specimens

Although the results obtained performing DIC analysis in comparison with the results obtained using LVDTs are consistent excepting some values, it is necessary to fixed a certain limit where

the difference between the maximum and minimum displacement cannot go further. And if so, the result is not reliable, being not possible to consider it within the final evaluation and comparison between the different performances of the specimens. Hence, for this case, the limit in which this difference should be in is 1.57mm. On the figure 80 corresponding to the top and bottom location, are red highlighted the maximum and minimum points for each specimen, obtaining with these points the difference to stablish either the specimen is reliable or not.

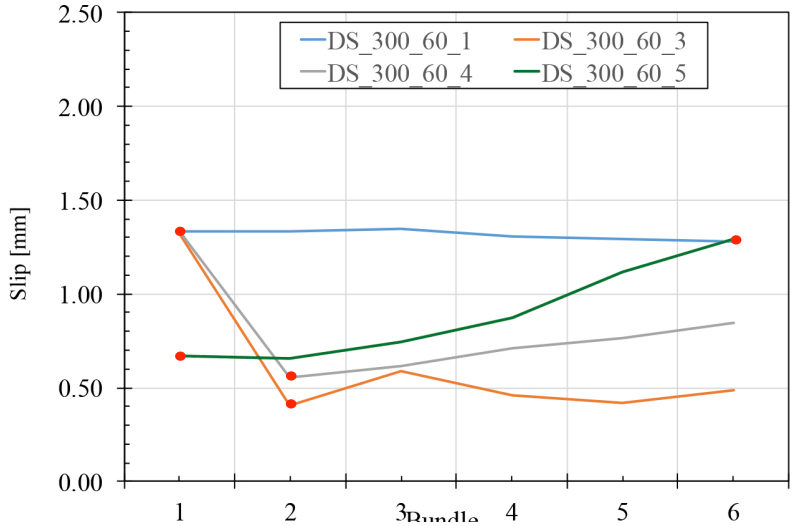

Figure 80 Slip at the top of the textile of all the specimens, highlighting the maximums and minimums

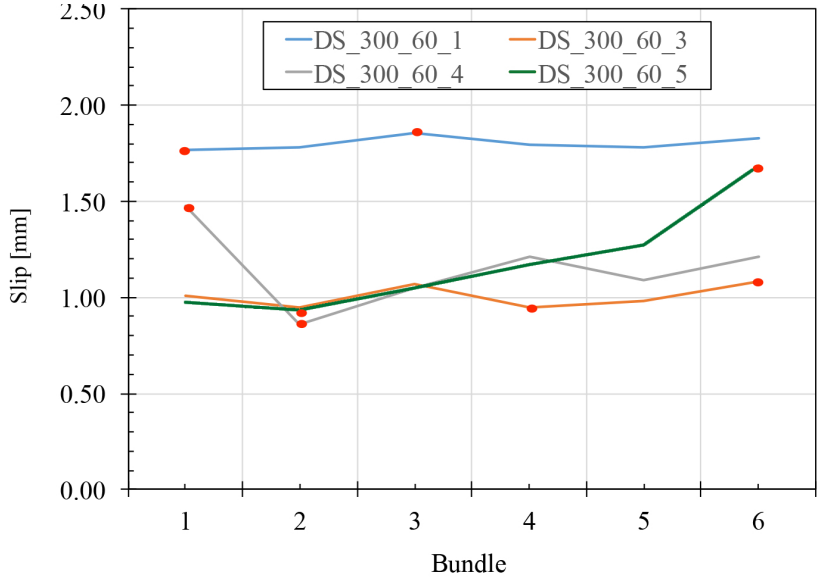

Figure 81 Slip at the bottom of the textile of all the specimens, highlighting the maximums and minimums

The results regarding to the difference between the maximum and minimum displacement of each specimen are reported on the table 9 and 10, where for both top and bottom the results are reliable. The fixed limit which defines the reliability of the results was defined based on the

fracture mechanics approach used for FRP-concrete joints exposed by (C. Carloni, 2014), extended later to the case of FRCM-concrete joints by (D´Antino, 2014).

Top			
specimen	Displacement [mm]		
	Maximum	Minimum	Difference
DS_300_60_1	1.348098877	1.276668323	0.071430554
DS_300_60_3	1.317316998	0.405403702	0.911913296
DS_300_60_4	1.33383436	0.557184972	0.776649388
DS_300_60_5	1.295603103	0.654578283	0.64102482

Table 10 Difference between the maximum and minimum slip registered at the top of the textile

Bottom			
specimen	Displacement [mm]		
	Maximum	Minimum	Difference
DS_300_60_1	1.852497939	1.767415273	0.085082666
DS_300_60_3	1.0801414	0.948076565	0.132064835
DS_300_60_4	1.474397153	0.860315553	0.6140816
DS_300_60_5	1.683153016	0.937089472	0.746063544

Table 11 Difference between the maximum and minimum slip registered at the bottom of the textile

In addition, is considerable important to analyse whether a more uniform distribution among the different bundles in the specimen may lead to a substantial increment in the ultimate strength or not. On the previous graph the specimen which exposed a more regular behaviour was DS_300_60_1, being at the same time the specimen supporting the lowest ultimate strength according to the results showed in the figure 82. Whereas specimen DS_300_60_1 reached the lowest ultimate strength, obviating the results regarding to the bundle five in the specimen DS_300_60_5, the specimen that reached the highest ultimate strength was DS_300_60_4 in which the distribution according to the figure 82 is much less uniform than the one seen in DS_300_60_1.

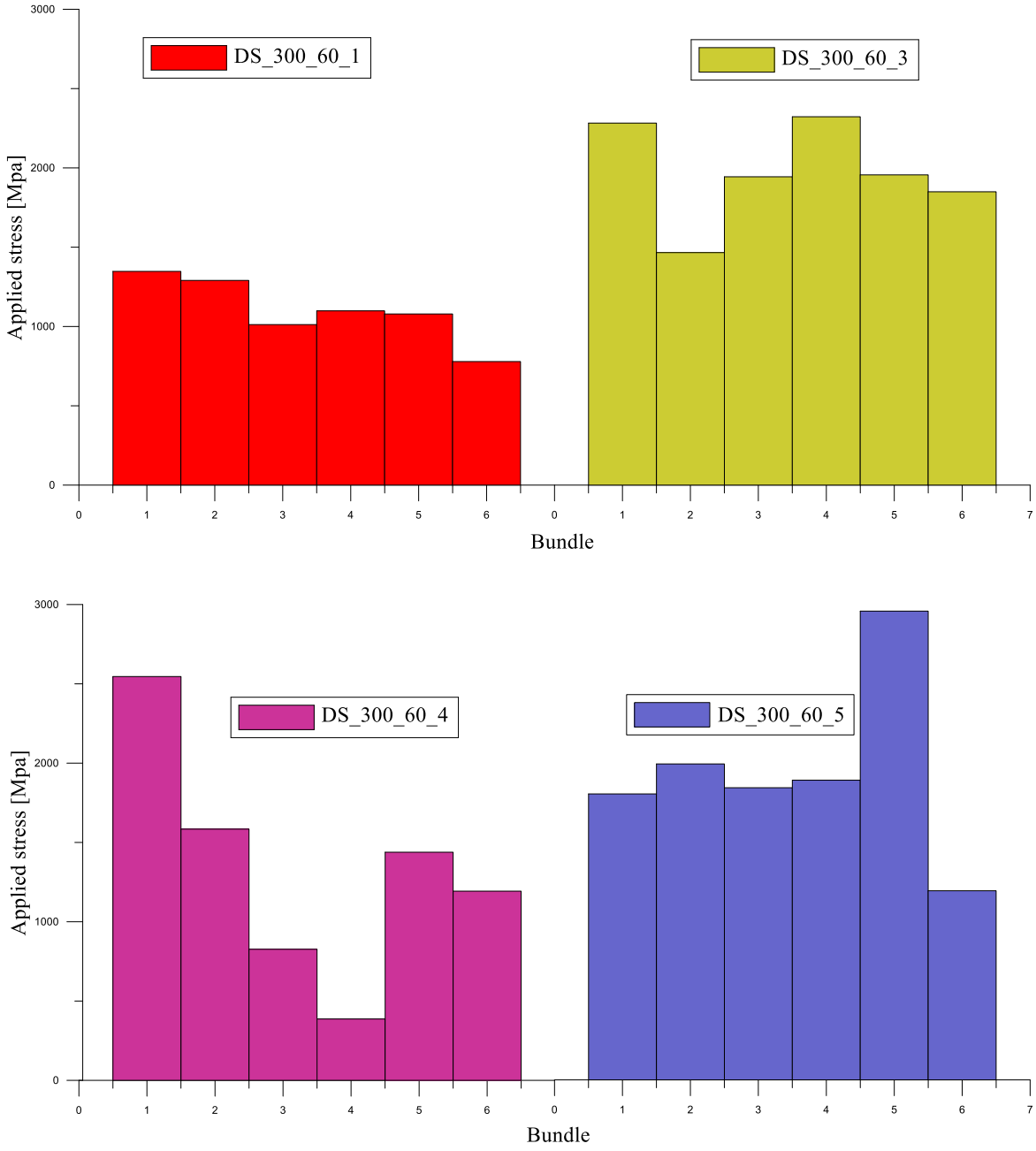

Figure 82 Final comparison between all the specimens in terms of stress-distribution

Concluding, it is worth to perform the comparison, in terms of strain and slip, between the different bundles according to their load distribution. On figure 83 is simultaneously plotted the results in terms of slip and strain, evidencing the highest displacement on the first specimen (DS_300_60_1), which was close to 2mm. Hence, theoretically the first specimen should experiment the less strain

compare to the others. This can be observed on the bottom part of the figure 83 and corroborated comparing to the bottom part of the figure 84, where is clear the strain experimented by specimen DS_300_60_1, being the lowest.

In some zones, certain peaks are present and are higher than the normal tendency due mainly to some difficulties of correlation that can be attributed to the software robustness during the data processing execution, but in general words the relation between strain and slip was kept, being the specimens subjected to a high slip, experimenting the lowest strain.

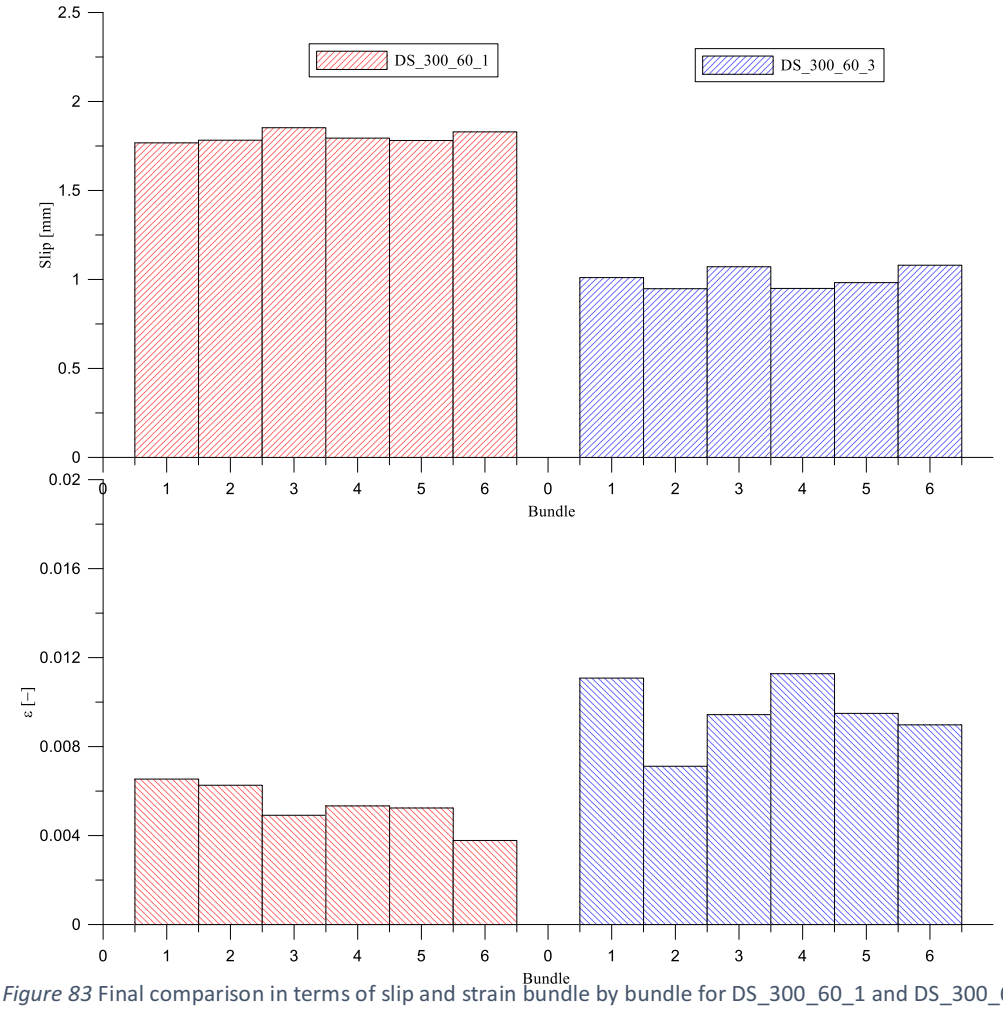

Figure 83 Final comparison in terms of slip and strain bundle by bundle for DS_300_60_1 and DS_300_60_3

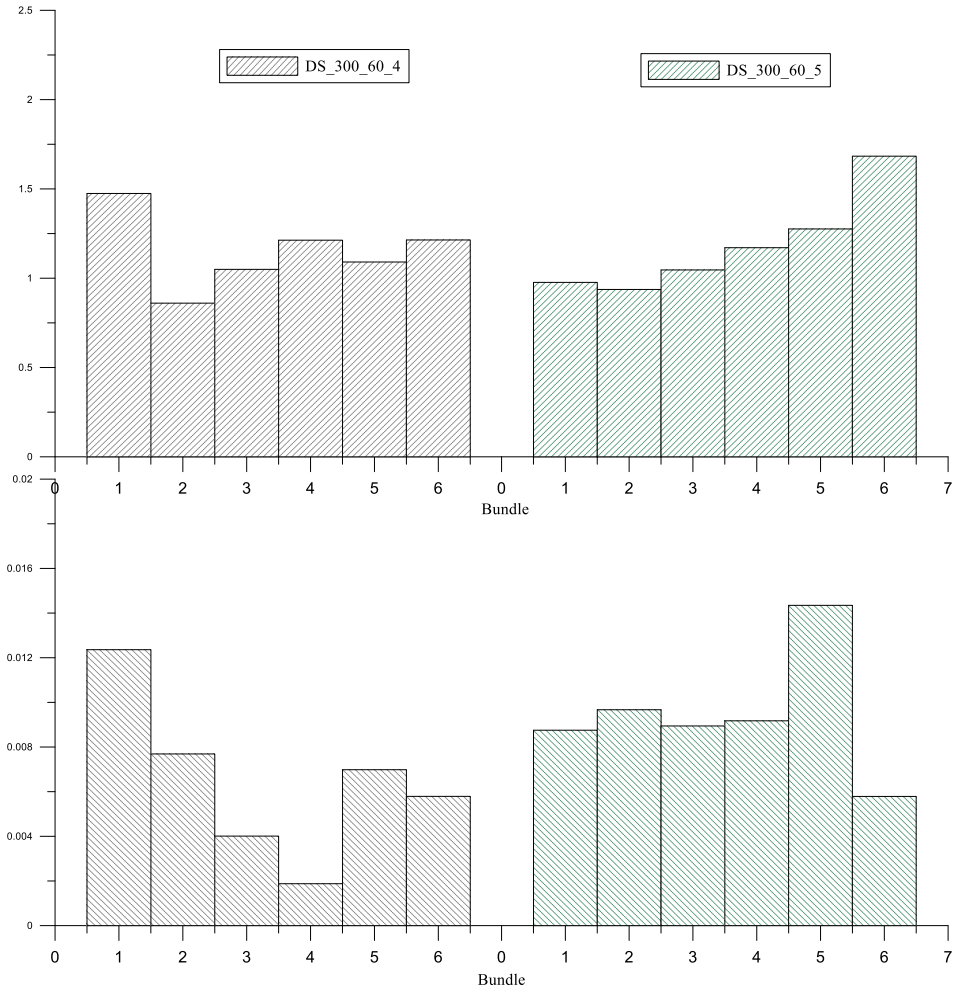

Figure 84 Final comparison in terms of slip and strain bundle by bundle for DS_300_60_4 and DS_300_60_5

5. CONCLUSIONS

Once the part regarding to the experimental campaign was finish, the results and its corresponding analysis and discussion were performed, in which the main objective of the thesis, being the study of the bonding behavior in FRCMs, was covered. Outstanding features came as results as the non-uniform load distribution among the bundles of each textile, being a repetitive factor observed within the results obtained from all the specimens.
This pattern observed repeatedly was observed more clear when the Digital Image Correlation analysis (DIC) was performed, where the load that each bundle within the textile was subjected to could be discretized respect the others, evidencing a differentiation in terms of load distribution along the textile. The results can be summarized on the figures 83 and 84, where the data is expressed in terms of slip and strain.

Being the non-uniform load distribution a common pattern during the execution of the different test, was necessary to proceed with an analysis in which the uniformity of the load distribution within the textile would be considered, becoming a new parameter to be evaluated regarding to the ultimate strength achieved. As an outcome, was concluded that the way how the load was re-distributed among the different bundles, being in some cases more uniform compared to other specimens, does not affect the overall performance. Moreover, analyzing the different results, within the non-uniformity load distribution, there was no a clear pattern, experimenting some specimens considerable high load peaks at some bundles while in other specimens the load was considerable more uniformly distributed, and this may be due mainly to the impregnation grade of the matrix within the textile. This impregnation grade can play a key role in the bond behavior of the FRCM, being at matrix/textile interface the place where the debonding occurs. Concluding with this that as more the impregnation grade of the matrix within the different bundles of the textile is, better the general bonding behavior would be.

On the other hand, another main parameter considered during the job, was the impact on the final performance that could have the way of casting of the different specimens. Regarding to PBO-FRCM was evident that this factor does not affect clearly on the overall performance of the specimens in terms of ultimate strength. Unlike PBO, in the use of steel fibers the way of casting plays a key role, resulting in a raise of approximately 15% in the ultimate strength, and it is due to the nature of the steel fibers, being considerable heavier than PBO, being more sensible when they are being casted.

Finalizing, and in order to standardize properly the overall procedure, it is recommended to control the measures when the FRCMs are made, optimizing the grade of impregnation of the matrix in the textile, guaranteeing with this a better performance when the FRCMs are applied on the substrate, being the matrix/textile interface the most critical in terms of bond behavior.

Bibliography

Adel Younis, U. E. (2018). *ELSEVIER.* Retrieved from https://ac.els-cdn.com/S095006181831033X/1-s2.0-S095006181831033X-main.pdf?_tid=9a81e85f-4b75-41df-a1fe-24708507776b&acdnat=1525966330_8d33d1a4f31463a2f920e947092e9bb6

Alecci V, D. S. (2016). *Experimental investigation on bond behavior of cement-based composites for strengthening of masonry structures.*

Ascione L, d. F. (2015). *Qualification method for externally bonded fiber reinforced cementitious matrix (FRCM) strengthening systems .*

Banholzer, B. (2004). *Bond behavior of multi-filament yarn embedded in a cementitious matrix.* Rheinisch-Westfälische Technische Hochschule (RETH).

Barbero, E. J. (n.d.). *Introduction to composite materials design .* CRC Press.

Bianchi, G. (n.d.). *Mechanical characterization of fabric reinforced cementitious matrix (FRCM) materials for structural strenghtening .* Giuseppe Bianchi .

C. Carloni, T. D. (2014). *Role of the matrix layers in the stress-transfer mechanism of FRCM composites bonded to a concrete substrate.*

C. Sabau, J. H. (2017). *Use of image correlation system to study the bond behavior of FRCM-concrete joints .*

Carozzi FG, M. G. (2014). *Mechanical properties and numerical modeling of fabric reinforced cementitious matrix (FRCM) systems for strengthening of masonry structures .*

Carozzi, F. G. (2016). *Mechanical characterization and bond behaviour of fibre reinforced cementitious matrix materials for strengthening of masonry buildings .*

Carrara, P. a. (2013). *A finite-difference model with mixed interface laws for shear tests of FRP plates bonded to concrete.*

Carrara, P. F. (2011). *Shear tests of carbon fiber plates bonded to concrete with control of snap-back.*

D´Ambrisi, A. a. (2011). *Flexural strengthening of RC beams with cement-based composites.*

D´Ambrisi, A. F. (2012). *Bond-slip relations for PBO-FRCM materials externally bonded to concrete.*

D´Ambrisi, A. F. (2013). *Experimental analysis on bond between PBO-FRCM strengthening materials and concrete.*

D´Ambrisi, A. F. (2013). *Strengthening of masonry-unreinforced concrete railway bridges with PBO-FRCM materials .*

D´Antino T, S. L. (2015). *Influence of the substrate characteristics on the bond behavior of PBO FRCM-concrete joints .*

D´Antino, T. (2014). *Bond behavior in fiber reinforced polymer composites and fiber reinforced cementitious matrix composites .*

Donnini, J. (2017). *ELSEVIER.* Retrieved from ELSEVIER: https://ac.els-cdn.com/S095006181730702X/1-s2.0-S095006181730702X-main.pdf?_tid=6707daa4-9ede-4a6b-9af7-5911e51b3d38&acdnat=1525945830_eeeeb2b5f05dabe64bf5dd665e4bd873

El-Hacha, R. (1997). *Strengthening of concrete members with advanced composite materials.* Concordia University, Montreal.

F. Ceroni, P. S. (n.d.). *ELSEVIER.* Retrieved from https://ac.els-cdn.com/S1359836817336247/1-s2.0-S1359836817336247-main.pdf?_tid=c9eee90a-5cd6-43ae-aef9-f0e84c90cdf4&acdnat=1526898653_0f428ff98f191b39d2a02702b7693509

Frances Giulia Carozzi, T. D. (2016). *ELSEVIER.* Retrieved from https://ac.els-cdn.com/S1359836816330657/1-s2.0-S1359836816330657-main.pdf?_tid=fff5ab99-97ea-41bf-8f5c-6b66e13accc0&acdnat=1525971477_db507011531f381ebaafb486e36c073e

Hadigheh SA, G. R. (2015). *Identification of the interfacial fracture mechanism in the FRP laminated substrates using a modified single lap shear test set-up .*

Kostiantyn Protchenko, M. W. (2015). *ELSEVIER.* Retrieved from https://ac.els-cdn.com/S1877705815013818/1-s2.0-S1877705815013818-main.pdf?_tid=5e3ecb71-9cb5-406e-b765-a2aaef11be01&acdnat=1526895259_b4b8637c73d82d4c7e22a36c4292fbcd

L, O. (2014). *Concrete confinement with a cement based high strength composite material.*

Lesley H. Sneed, S. V. (2016). *ELSEVIER.* Retrieved from https://ac.els-cdn.com/S0141029616305429/1-s2.0-S0141029616305429-main.pdf?_tid=b9328644-30ce-486a-94fc-e7ce142ea46f&acdnat=1528630743_f14a3ab3c5d8b5e3047d97bd4071afc2

Malena M, d. F. (2014). *Debonding of composites on a curve masonry substrate: experimental results and analytical formulation .*

Marcin Tekieli, S. D. (2016). *Application of digital image correlation to composite reinforcements testing.*

Nanni, A. E. (2014). Retrieved from https://www.scopus.com/record/display.uri?eid=2-s2.0-84924873288&origin=resultslist&sort=plf-f&src=s&st1=frcm+in+north+america&st2=&sid=1806dad331dad72accfbb3c1065b99cf&sot=b&sdt=b&sl=36&s=TITLE-ABS-KEY%28frcm+in+north+america%29&relpos=0&citeCnt=0&searchTerm=

Ombres L, V. S. (2015). *Structural behavior of fabric reinforced cementitious matrix (FRCM) strengthened concrete columns under eccentric loading.*

P, M. (2013). *Uncertainty estimation and reduction in digital image correlation measurements .*

Pellegrino C, D. T. (2013). Failure due to delimitation in concrete elements strengthened with cementitious composites . *8th international conference on fracture mechanics of concrete and concrete structures.*

Pilla, M. P. (2017). *Experimental and numerical analysis of the matrix-fibre bond behaviour of inorganic-matrix composites for structural strengthening .*

Sneed LH, V. S. (2016). *Flexural behavior of RC beams strengthened with steel-FRCM composite.*

Trapko, T. (2014). *ELSEVIER .* Retrieved from https://ac.els-cdn.com/S095006181401071X/1-s2.0-S095006181401071X-main.pdf?_tid=8affd917-2709-4233-8ba5-644857ccdf5e&acdnat=1528110669_22988786d9d5f663dd173f61aa381eaa